MECHANICAL PROPERTIES AND FATIGUE BEHAVIOR OF UNITIZED COMPOSITE AIRFRAME STRUCTURES AT ELEVATED TEMPERATURE

THESIS

Mohamed Noomen, Lieutenant, TNAF

AFIT-ENY-MS-16-S-66

DEPARTMENT OF THE AIR FORCE
AIR UNIVERSITY

AIR FORCE INSTITUTE OF TECHNOLOGY

Wright-Patterson Air Force Base, Ohio

(IF your document is limited, place your Destruction Notice Here)

AFIT-ENY-16-S-66

MECHANICAL PROPERTIES AND FATIGUE BEHAVIOR OF UNITIZED COMPOSITE AIRFRAME STRUCTURES AT ELEVATED TEMPERATURE

THESIS

Presented to the Faculty

Department of Aeronautics and Astronautics

Graduate School of Engineering and Management

Air Force Institute of Technology

Air University

Air Education and Training Command

In Partial Fulfillment of the Requirements for the

Degree of Master of Science in Aeronautical Engineering

Mohamed Noomen, B.S.M.E

Lieutenant, TNAF

September 2016

AFIT-ENY-16-S-66

MECHANICAL PROPERTIES AND FATIGUE BEHAVIOR OF UNITIZED COMPOSITE AIRFRAME STRUCTURES AT ELEVATED TEMPERATURE

Mohamed Noomen, B.S.M.E

Lieutenant, TNAF

Committee Membership:

Dr. Marina B. Ruggles-Wrenn, PhD
Chair

Dr. Thomas G. Eason III, PhD
Member

Lt Col Sheena Winder, PhD
Member

Abstract

The tension-tension fatigue behavior of a newly developed unitized composite material system was investigated. The unitized composite consisted of a polymer matrix composite (PMC) co-cured with a ceramic matrix composite (CMC). The PMC portion consisted of an NRPE high-temperature polyimide matrix reinforced with carbon fibers woven in an eight harness satin weave (8HSW). The CMC layer is a singly-ply non-crimp 3D orthogonal weave composite consisting of a ceramic matrix reinforced with glass fibers. In order to assess the performance and suitability of this composite for use in aerospace components designed to contain high-temperature environments, mechanical tests were performed under temperature conditions simulating the actual operating conditions. In all elevated temperature tests the CMC side of the test specimen was at 329°C while the PMC side was exposed to ambient laboratory air. The tensile properties were measured at elevated temperature for both on-axis [0/90] and off-axis [±45] fiber orientations. Tension-tension fatigue tests were conducted at elevated temperature at a frequency of 1.0 Hz with a ratio of minimum stress to maximum stress of R= 0.05. Fatigue run-out for this effort was defined as 2×10^5 cycles. Both strain accumulation and modulus evolution during cycling were analyzed for each fatigue test. Specimens which achieved fatigue run-out were subjected to tensile tests to failure in order to characterize the retained tensile properties. Microstructural investigation of tested specimens revealed different degrees of delamination in the material system depending on the fiber orientation and fatigue stress levels.

Acknowledgments

First and foremost, I would like to thank Allah. I would also like to gratefully thank my advisor, Dr. Marina Ruggles-Wrenn, for her guidance and countless hours of support and guidance. In addition, I would also like to thank Dr. Thomas Eason (AFRL/RQHF) and Dr. Sheena Winder (AFRL/RXAN) for their time and support. I would also like to thank the AFIT/ENY laboratory technicians Mr. Barry Page, Mr. Jamie Smith, and Joshua Dewitt for their consistent support with lab equipment from training to maintaining. Thanks to my AFIT colleagues for making these two years, away from home, a wonderful and unforgettable experience.

Last but not the least, Thanks to Mrs. Annette Robb for always being there for her international officers, the work you do and the endless support are not forgotten.

Table of Contents

Page

List of Figures

Page

List of Tables

Page

Nomenclature

σ	Stress
E	Young's modulus (GPa)

List of Acronyms

2D	Two Dimensional
3D	Three Dimensional
AFIT	Air Force Institute of Technology
AFRL	Air Force Laboratory
CMC	Ceramic Matrix Composite
HTPMC	High Temperature Polymer Matrix Composite
MS	Material System
MTS	Material System Test
PMC	Polymer Matrix Composite
SiC	Silicon Carbide
UTS	Ultimate Tensile Stress

MECHANICAL PROPERTIES AND FATIGUE BEHAVIOR OF UNITIZED COMPOSITE AIRFRAME STRUCTURES AT ELEVATED TEMPERATURE

I. Introduction

The use of composite materials in the aerospace industry has greatly increased in the recent decades. These material systems offer light weight combined with improved fatigue performance, excellent thermal resistance and damage tolerance. In existing and future Air Force systems, different airframe structures and components that operate at elevated temperatures utilize composite materials. Figure 1 shows the growing use of composite materials in aircraft structures.

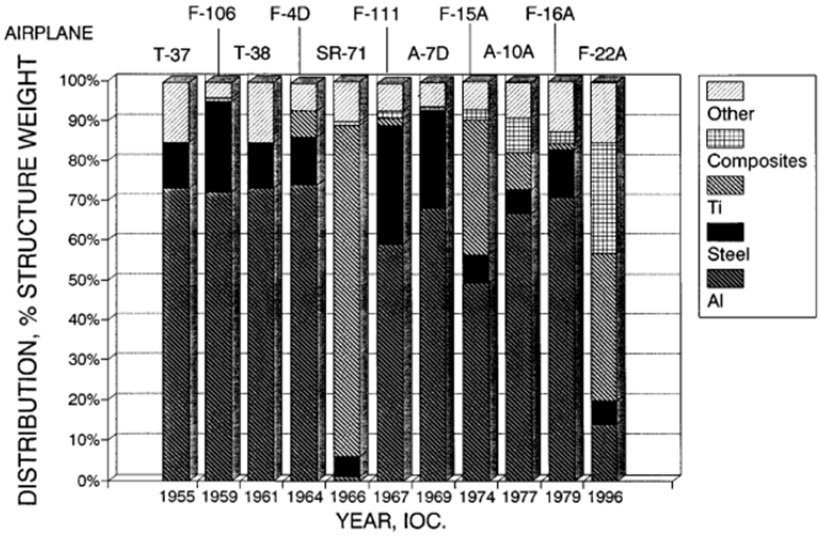

Figure 1. Use of different materials in aircraft structures over time. [1]

Polymer matrix composites (PMCs) and ceramic matrix composites (CMCs) are two types of composites used in aircraft structures intended to operate at high

temperatures. The PMR-15 resin is widely used as matrix material for high temperature polymer matrix composites (HTPMCs) in the aerospace industry. However, research efforts to develop replacement polyimide resins are ongoing, mainly due to carcinogenic elements in PMR-15 [2]. Recently, the Performance Polymer Solutions Inc. ($P^2SI^®$) of Moraine, Ohio developed a polyimide NRPE resin as a possible replacement for PMR-15. This newly developed NRPE resin was used as a matrix material in the unitized composite material system studied in this work.

In aircraft application, HTPMCs are being considered for use in structural components that must operate in the "hot zone". Frequently, temperatures in the "hot zone" exceed the maximum operating temperatures of the HTPMCs. Thermal protection systems (TPS) are being developed specifically to shield the HTPMC components from excessive temperatures. The unitized PMC/CMC composite studied in this work was designed specifically to operate as a thermal protection system where a CMC layer serves as a thermal barrier for the PMC. For successful application of the unitized PMC/CMC composite material system in advanced aerospace systems, it is critical that mechanical properties and mechanical behavior of this material be thoroughly understood.

The objective of this work was to assess the performance and suitability of the unitized PMC/CMC composite for use in aerospace components subjected to contain high-temperature environments. In order to simulate actual operating conditions, mechanical tests were performed with the CMC of the specimen subjected to a temperature of 329°C while the PMC side was open to ambient laboratory air. Monotonic tensile tests to failure conducted in order to measure the baseline tensile properties. Fatigue performance was assessed in tension-tension fatigue tests. The experimental

program targets both fiber-dominated and matrix-dominated mechanical properties and behavior.

The following tasks were performed to achieve the research objectives:

1. Elastic modulus of each specimen was determined at room temperature in order to assess specimen-to-specimen variability.
2. Monotonic tensile tests to failure were performed in order to assess tensile stress-strain behavior and to determine tensile properties for both 0/90 and ±45 fiber orientations at elevated temperature.
3. Tension-tension fatigue tests were performed to evaluate fatigue behavior for both 0/90 and±45 fiber orientations at elevated temperature. Based on experimental data fatigue S-N curves were constructed and fatigue limits corresponding to the run-out condition of 2×10^5 cycles were determined.
4. Tested specimens were examined under optical microscope in order to elucidate damage and failure mechanisms.

II. Background

2.1 Composite Materials

A composite is a material consisting of two or more materials. Composites are designed to exhibit properties and/or performance superior to those of the constituent materials. Composites are typically comprised of a matrix and a dispersed phase called reinforcement. The reinforcement phase can be particulates, whiskers, or fibers. Its main purpose is to bear the load and to provide the strength and the stiffness.

The matrix phase is continuous and can be made from polymers, metals, or ceramics. Matrix keeps the fibers in the proper architecture and protects them from abrasion. Furthermore, in the case of polymer and metal matrix composites which exhibit a strong bond between the fiber and the matrix, the matrix transmits shear loading at the fiber/matrix interface [5]. Fibers (unidirectional or as a woven fabric) and matrix arranged in one layer form a lamina or ply. A laminate consists of multiple plies organized together. Individual plies may have different fibers orientations. Figure 2 shows a schematic of a laminated composite material. One of the failure modes encountered in laminated composites is inter-laminar separation, also known also as delamination. This failure mode may interact with transverse cracking during the failure process [6].

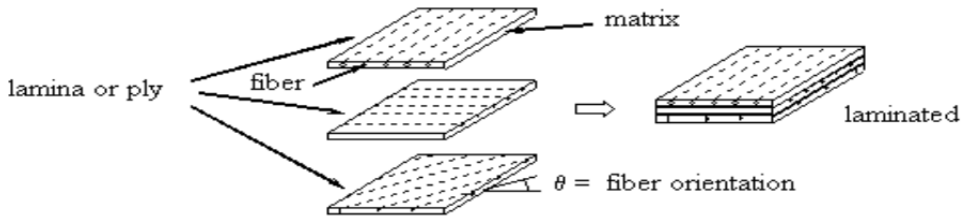

Figure 2. Laminated Composite Materials [7]

2.2 Polymer Matrix Composites

Matrix materials used in PMCs can be divided into two categories: thermoplastic and thermoset. The thermoplastic resins include polyesters, poly-etherimide, polyamide imide, polyphenylene sulfide, polyether-etherketone (PEEK), and liquid crystal polymers. Thermoplastic resins are melted to a viscous liquid at high processing temperature, formed into desired shape, then cooled. The manufacturing process is reversible; the thermoplastic can be reshaped by simply reheating. In contrast, thermoset resins that include polyesters, vinyl-esters, epoxies, and polyamides are produced by an irreversible curing process. This process relies on chemical reactions that crosslink the polymer chains into a three dimensional network. Figure 3 shows a comparison of general characteristics of thermoset and thermoplastic matrix materials [8].

Resin type	Process temperature	Process time	Use temperature	Solvent resistance	Toughness
Thermoset	Low	High	High	High	Low
Toughened thermoset	↑	↓	↑	↑	↓
Lightly crosslinked thermoplastic	↑	↓	↑	↑	↓
Thermoplastic	High	Low	Low	Low	High

SOURCE: Darrel R. Tenney, NASA Langley Research Center.

Figure 3. Comparison of general characteristics of thermosets and thermoplastics. Reproduced from [8]

The reinforcement phase provides strength and stiffness of the composite. Glass, carbon, silicon carbide (SiC), and aramid are typically used as reinforcement materials in PMCs [9].

2.3 Ceramic Matrix Composites

Ceramic matrix composites consist of ceramic fibers embedded in a ceramic matrix. Ceramic matrix composites can be divided into two separate categories:

oxide/oxide CMCs such as Al_2O_3/Al_2O_3 and non-oxide CMCs, such as C/C, C/SiC, or SiC/SiC [10]. Ceramics combine high stiffness with low density while operating over a wide range of temperatures. However, monolithic ceramics are brittle, exhibit low toughness and are prone to catastrophic failure. Ceramic matrix composites, which exhibit improved damage tolerance and graceful failure, were developed specifically to combat the low toughness and propensity for catastrophic failure of the monolithic ceramics [5]. In the case of PMCs, a strong bond between the fibers and the matrix is needed to transmit load from the matrix to the fibers through shear loading at the interface. In contrast, in the case of the CMC, a weak fiber/matrix interface is needed to increase toughness and damage tolerance [5].

2.4 2D vs 3D Reinforcement

A common technique employed to produce the reinforcement for composite materials is a 2D weaving process. This process utilizes two mutually orthogonal sets of yarns called weft in the transverse direction and warp in the longitudinal direction of the fabric. Recently a further improvement was achieved by implementing a 3D weaving process that includes mutually orthogonal sets of wefts arranged with a set of warps. This process was introduced to increase the strength in the through-thickness direction of the composite and to improve delamination resistance. However, the 3D weaving process can introduce additional internal defects and lower the in-plane properties such as the strength and stiffness [11]. A schematic of a non-crimp 3D orthogonal weave is shown in Figure 4.

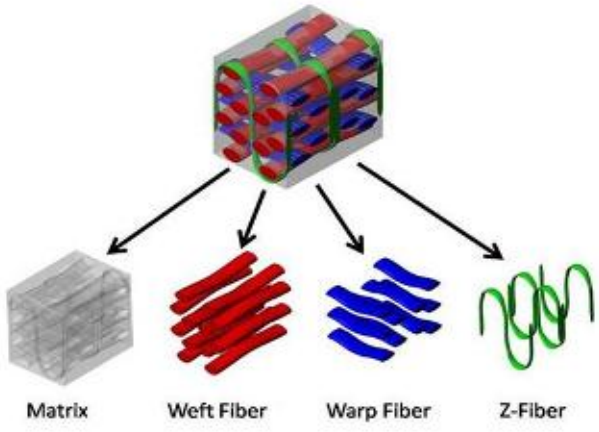

Figure 4. Schematic of a non-crimp 3D orthogonal weave [12].

2.5 Previous Research on Unitized PMC/CMC Composites

The co-cured unitized composite is a novel material system that is yet to be thoroughly investigated. However, similar material systems have been researched. Consider, for example, fiber metal Laminates (FMLs) consisting of a self-reinforced polypropylene (SRPP) composite and an aluminum alloy. The FMLs are designed to combine the energy absorbing characteristics of thermoplastic matrix composites with the strength and stiffness of metals [13]. Recently at AFIT, Wilkinson [3] evaluated tensile properties and studied tension-tension fatigue behavior of a 2D PMC/CMC unitized composite comprised of constituents similar to those of the unitized composite studied in this work. A brief description of the 2D PMC/CMC unitized composite studied by Wilkinson is provided in the Appendix A. Results obtained by Wilkinson in tension-to-failure tests are summarized in Tables 1 and 2. Wilkinson observed that the addition of the CMC layer did not offer an improvement in strength or in stiffness at room or at elevated temperature. Wilkinson reported that the 2D PMC (which had the same constituent materials and the same fiber architecture as the PMC portion of the 2D

PMC/3D CMC) exhibited greater strength than the 2D PMC/CMC unitized composite for both 0/90 and ±45 fiber orientations. The ±45 modulus of the 2D PMC was greater than that of the 2D PMC/CMC unitized composite, while the 0/90 modulus of the two material systems was roughly the same. Results obtained by Wilkinson in tension-tension fatigue tests are summarized in Tables 3 and 4. Wilkinson demonstrated that the 2D PMC offered an overall better fatigue performance than the unitized 2D PMC/CMC, especially at higher cyclic stress levels.

Note that the unitized composite studied in this work has the same matrix and reinforcement materials as the 2D PMC and the 2D PMC/CMC studied by Wilkinson. Hence, the results obtained in this work are compared to the results reported by Wilkinson in order to determine whether the unitized 2D-PMC/3D-CMC material system offers an improved mechanical performance.

Table 1. Summary of tensile properties obtained for 2D PMC/CMC at room temperature and elevated temperature (T_{right} = 329°C). Data from Wilkinson [3].

Material System 3: 2D PMC/CMC

Fiber Orientation	Specimen #	Elastic Modulus (GPa)	Normalized Modulus (GPa)	UTS (MPa)	Normalized UTS (MPa)	Failure Strain, ϵ_f (%)
0/90°	*Room Temperature:*					
	T5-1	54.03	55.93	643.3	665.8	1.918
	T5-2	56.84	56.85	654.8	654.8	1.291
	T5-3	55.97	57.77	703.1	725.7	1.275
	Elevated Temperature:					
	T5-4	56.06	56.49	669.0	674.2	1.161
	T5-5	60.43	61.27	660.8	669.9	1.382
	T5-6	59.08	55.81	686.7	648.7	1.059
±45°	*Room Temperature:*					
	T6-1	11.45	10.76	61.7	58.0	1.390
	Elevated Temperature:					
	T6-2	9.41	9.39	57.1	57.0	2.131
	T6-3	9.38	9.06	57.7	55.7	2.947

Table 2. Summary of tensile properties for 2D PMC at room temperature and elevated temperature (T_{right} = 329°C). Data from Wilkinson [3].

Material System 2: 2D PMC

Fiber Orientation	Specimen #	Elastic Modulus (GPa)	Normalized Modulus (GPa)	UTS (MPa)	Normalized UTS (MPa)	Failure Strain, ϵ_f (%)
0/90°	*Room Temperature:*					
	T1-1	56.87	57.29	831.8	837.9	1.401
	Elevated Temperature:					
	T1-2	60.93	61.88	834.4	847.3	1.276
	T1-6	59.04	58.03	809.6	795.7	1.287
±45°	*Room Temperature:*					
	T2-1	16.65	16.47	165.1	163.3	6.118
	Elevated Temperature:					
	T2-2	13.67	13.48	128.3	126.4	12.955*

** Failure strain taken at point where stress dropped to 50% UTS.*

Table 3. Tension-tension fatigue results for 2D PMC/CMC at elevated temperature (T_{right} = 329°C). Data from Wilkinson [3].

Specimen #	Maximum Stress (MPa)	Maximum Stress (% UTS)	Normalized Max. Stress (MPa)	Normalized Max. Stress (% Norm. UTS)	Cycles to Failure (N)	Failure Strain (%)
0/90° Fiber Orientation						
T5-18	572.1	85	579.5	87	61	0.400
T5-16	572.6	85	557.3	84	297	0.325
T5-10	539.4	80	542.4	82	3,630	0.160
T5-13	538.7	80	532.5	80	425	0.162
T5-8	539.2	80	530.3	80	21,327	0.502
T5-14	505.4	75	520.7	78	190,580	0.397
T5-17	518.9	77	520.5	78	61,787	0.138
T5-9	505.1	75	508.9	77	4,152	0.631
T5-11	505.3	75	499.5	75	102,523	0.453
T5-7	471.8	70	471.7	71	200,000[a]	-0.165[a,b]
±45° Fiber Orientation						
T6-14	48.2	84	48.4	86	220	1.126
T6-12	46.5	81	46.7	83	664	1.345
T6-6	46.8	82	45.7	81	805	1.370
T6-11	41.2	72	42.5	75	5,604	1.564
T6-4	43.7	76	42.3	75	2,108	1.300
T6-7	41.3	72	41.4	73	3,972	1.259
T6-13	39.9	70	40.1	71	1,894	0.728
T6-8	38.7	67	39.2	70	40,423	1.420
T6-10	37.6	65	38.7	69	65,598	1.702
T6-9	35.7	62	35.7	63	185,365	1.022
T6-5	32.9	57	32.4	58	200,000[a]	0.327[a]

[a] Run-out; defined as 2×10^5 cycles. Failure of specimen did not occur when the test was terminated.
[b] Anomalous strain value.

Table 4. Tension-tension fatigue results for 2D PMC at elevated temperature (T_{right} = 329°C). Data from Wilkinson [3].

Specimen #	Maximum Stress (MPa)	Maximum Stress (% UTS)	Normalized Max. Stress (MPa)	Normalized Max. Stress (% Norm. UTS)	Cycles to Failure (N)	Failure Strain (%)
0/90° Fiber Orientation						
T1-5	740.1	90	759.7	92	2,756	0.130
T1-12	740.8	90	734.3	89	1,148	1.649
T1-11	723.9	88	719.8	88	10,916	—
T1-8	699.6	85	683.7	83	11,286	0.308
T1-3	658.0	80	663.0	81	23,768	1.111
T1-10	618.4	75	610.2	74	121,136	0.787
T1-7	576.3	70	585.3	71	200,000[a]	0.057[a]
T1-4	494.5	60	503.3	61	200,000[a]	0.167[a]
±45° Fiber Orientation						
T2-8	105.8	82	100.5	79	917	5.749
T2-7	94.0	73	99.0	78	2,291	6.434
T2-4	99.8	78	97.3	77	793	7.013
T2-6	87.6	68	89.2	71	4,888	7.183
T2-9	81.7	64	82.6	65	20,941	6.323
T2-3	75.7	59	76.1	60	102,372	7.050
T2-11	69.7	54	69.4	55	200,000[a]	1.471[a]
T2-5	63.4	49	66.4	53	200,000[a]	0.611[a]

[a] *Run-out; defined as 2×10^5 cycles. Failure of specimen did not occur when the test was terminated.*
[b] *Anomalous strain value.*

III. Material and Test Specimen

This section discusses the material system investigated in this research effort, test specimen geometry, and test specimen preparation.

3.1 Unitized PMC/CMC Composite Material System

The unitized composite material system consists of a 2D PMC and a 3D CMC co-cured together. The purpose of combining these two types of composites together is to create a unitized material with a CMC layer that acts as a thermal barrier for the PMC. The 2D PMC part consists of a P^{2}SI® NRPE matrix reinforced with 12 plies of de-sized Cytec T650-35 carbon fibers woven in an eight harness satin weave (8HSW). The P^{2}SI® NRPE matrix material, developed by Performance Polymer Solutions Inc. (P^{2}SI/PROOF Research, Moraine, OH, USA) is a high-temperature structural thermosetting polyimide resin. The P^{2}SI® NRPE resin exhibits low-melt viscosity compared to PMR-15 and is expected to maintain its structural integrity after continuous exposures at temperatures up to 343 °C [14].

The 3D CMC portion consists of a ceramic matrix reinforced with AGY S-2 glass fibers in a non-crimp 3D orthogonal weave. A schematic of a non-crimp 3D orthogonal weave is shown in Figure 6.The ceramic matrix was produced using StarPCSTM SMP-730 pre-ceramic resin. StarPCSTM SMP-730 is a polycarbosilane precursor to thermally stable silicon carbide. SMP-730 polymer can be used as a thermoplastic resin at low temperatures. Upon heating to higher temperatures the polymer cures to a thermoset solid. The cured polymer can then be fired to form a high temperature, oxidation resistant, amorphous silicon carbide material [15]. The S-2 fiber manufactured by AGY®

is based on magnesium aluminosilicate glasses. The S-2 fiber exhibits high strength, modulus, and stability under extreme temperature and corrosive environments [16]. The use of 3D reinforcement is expected to improve delamination resistance of the CMC part. Details of the 3D glass fiber fabric are summarized in Table 5.

Table 5. Details of the three-dimensional fabric design. Data provided by Performance Polymer Solutions Inc. (P2SI/PROOF Research, Moraine, OH, USA).

No. Warp Layers	dpi[1]	No. Fills	ppi[2]	Warps (%)	Fills (%)	Z (%)	h (mm)	V_f (%)
2	8.0	3	4.4	40.3	39.9	19.8	1.7-2.0	47.9

[1] dents per inch (dent – space between the wires of a reed on a loom through which the warp yarns pass)
[2] picks per inch (pick – single fiber yarn pulled through a weave)

The co-curing process used to fabricate the unitized PMC/CMC composite is proprietary. Because the unitized PMC/CMC consists of two dissimilar materials, physical properties of PMC/CMC panels such as constituent content percentages could not be readily measured. The overall thickness of the PMC/CMC specimens was approximately 5.5 mm. The average thickness of the PMC part was approximately 4.5 mm, while the average thickness of the CMC part was approximately 1 mm. Hence, the plane of PMC/CMC co-curing is not located at the mid-plane of the unitized PMC/CMC composite panel.

3.2 Specimen Geometry

To ensure that failure occurred within the gage section of the test specimen standard dog bone-shaped specimens were used for all monotonic tension tests and tension-tension fatigue tests. The specimen geometry is presented in Figure 5.

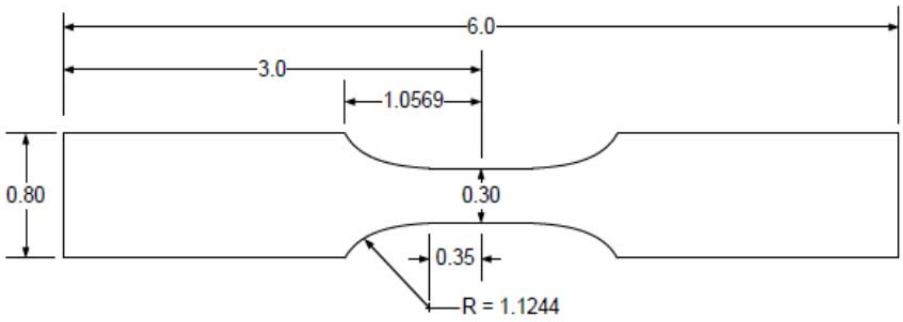

Figure 5: Tension-tension specimen geometry, all dimensions in inches

3.3 Specimen Preparation

The AFIT Model and Fabrication shop used diamond-grinding to machine test specimens from composite panels. The first panel of the material system was cut into specimens with 0/90 fiber orientation. The second panel was cut into specimens with ±45 fiber orientation for characterization of the off-axis material performance. Then each specimen was labeled. The specimen labels refer to specimen geometry, material system and fiber orientation. For example, T7-1 refers to tensile specimen number 1 with 0/90 fiber orientation cut from a panel of the 2D PMC/ 3D CMC (panel MS4-1). Specimen labels corresponding to the material system and fiber orientations can be seen in Table 6.

Table 6. Specimen labeling scheme

Material System	Material Type & Fiber Weave	Panel ID	Fiber Orientation	Label	Example Specimen Labels	Number of Specimens
MS4	2D PMC/ 3D CMC	MS4-1	[0/90]	T7	T7-1	20
		MS4-2	[±45]	T8	T8-5	15

The gage section width and thickness were measured using a Mitutoyo Absolute Solar Digimatic Caliper, Model N0. CD-S6”CT. A slight variation in dimensions was noticed and documented upon measurement of specimens. Table 7 below gives the average test specimen dimensions.

Table 7. Average tension-tension specimen dimensions.

Material System	Panel	Fiber Orientation	Average Width (mm)	Average Thickness (mm)	Avg Cross-Sect. Area (mm^2)
MS4	1	[0/90]°	7.61	6.43	48.91
	2	[±45]°	7.62	6.26	47.73

In order to remove contaminants from the machining process the specimens were cleaned with a solution of soap and water and rinsed with distilled water. Then, they were dried in an Isotemp Model 282A vacuum oven set to 105°C and approximately 2 in. Hg pressure. After drying, the specimens were stored at room temperature in a desiccator.

Prior to testing two dimples were created in the side of the specimen to ensure continuous contact between the specimen and the extension rods of the axial extensometer. Note that the dimples were positioned in the PMC portion and were kept to a minimal depth to avoid fracture initiation. In addition, fiberglass tabs of 1/16’’ thickness were attached to the top and bottom surfaces of the specimen in order to

prevent the wedge surface from damaging the specimen and to transfer the load. The tabs were bonded to the specimen using the M-bond 200 adhesive. Figure 6 shows a test specimen with fiberglass tabs bonded to the specimen gripping sections.

.

Figure 6. Unitized composite specimen with fiberglass tabs

IV Experimental Setup and Test Procedures

This section provides a description of the equipment and test setup, temperature calibration procedure and mechanical test procedures used in this research.

4.1 Mechanical Testing Equipment

The 810 MTS servo-hydraulic testing machine with a 100 kN (22 kip) model 647.10A load cell and MTS model 647.10 water-cooled hydraulic wedge grips was used in all tests performed in this work. The grip pressure was set to 10 MPa. The strain measurement was performed using an MTS model 632.53E-14 axial extensometer with a 12.7-mm gage section. The elevated temperature tests employed a single zone MTS 653 furnace equipped with an MTS 409.83 temperature controller. Figure 7 shows the testing machine, furnace, and extensometer. Flex Test 40 digital controller was used for data acquisition and input signal generation. The MTS station builder release 5.2B was used to create a configuration file while operations were controlled using the station manager interface. The testing procedures were developed to run each desired test and to collect data. Typically the following data were collected: force, force command, displacement, strain, test temperature, and time.

Figure 7. Testing facility.

4.2 Temperature Calibration

The CMC side of the unitized composite faced the furnace in all tests performed at elevated temperature. Therefore, a temperature calibration was performed to maintain a temperature of 329°C in the gage section on the CMC side of the specimen. Two K type thermocouples were attached to the specimen gage section with Kapton tape, one on the CMC side, and one on the PMC side (see Figure 8). The thermocouples were then connected to a hand-held Omega HH501DK temperature sensor for temperature read-out.

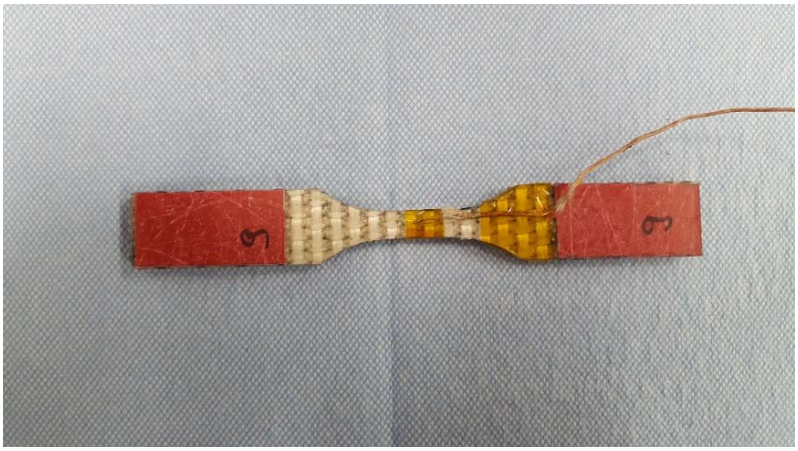

Figure 8: Temperature calibration specimen.

Furnace insulation inserts were shaped to fit the specimen geometry so as to direct the furnace heat to the CMC side and keep the PMC side of specimen open to ambient air. The insulation setup is shown in Figure 9.

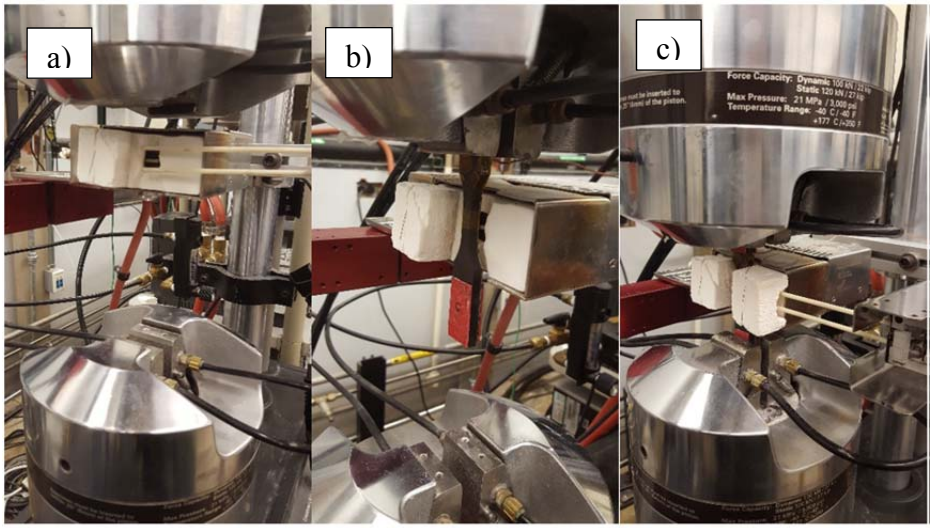

Figure 9. Furnace insulation setup: a) Back insert in place b) Specimen gripped c) Specimen ready for testing

A temperature calibration procedure was developed using MTS software; the temperature was ramped to an initial temperature at a rate of 10°C/min. Once initial temperature was reached the furnace temperature controller was adjusted manually until the temperature of the CMC side (right side) reached the desired test temperature of

329°C. The temperature controller was then kept at this set temperature for 3 hours to ensure that temperature of 329±5 °C could be consistently maintained. Temperature calibration procedure was performed separately for the 0/90 and ±45 specimens. Results revealed that the same temperature set point was required for testing specimens with both fiber orientations. The furnace temperature controller set points are shown in Table 8. Note that two set points are given. In the course of this work one of the insulation inserts had to be replaced. Then temperature calibration procedure was accomplished with a new insert.

Table 8. Furnace set point temperature for elevated temperature tests

Specimen Type	Furnace Set-point °C
MS4	605 / 535

4.3 Mechanical Test Procedures

4.3.1 Room Temperature Elastic Modulus Measurements.

The room temperature elastic modulus of each specimen was measured in order to assess specimen to specimen variability. The modulus measurement tests were performed in a stress control mode with a rate of 1 MPa/s. Each specimen was subjected to three cycles between zero stress and 20 MPa and the strain data were collected using the extensometer. For each loading and unloading segment, the modulus was determined as a slope of a best fit line on a stress-strain curve. Average modulus was obtained by considering modulus values determined from all segments.

4.3.2 Monotonic Tensile Tests.

The monotonic tension-to-failure tests were conducted with the CMC side of the specimen (right side) at an elevated temperature of 329°C and the PMC side exposed to ambient air. Two specimens of each fiber orientation were tested to determine the as-processed tensile properties and to assess the tensile stress-strain behavior.

The MTS software was used to develop the test procedures. The furnace temperature was first raised to the required set point at a rate of 10°C/min, and then kept constant for 45 min before the specimen was loaded in displacement control to failure. Displacement rate was 0.025 mm/s. Failure was considered to occur when the load supported by the specimen dropped dramatically. The following data were collected: force, displacement, displacement command, strain, temperature command, temperature, and time. The strain data collected during the temperature ramp up and dwell periods is considered the thermal strain.

4.3.3 Fatigue Tests.

The tension-tension fatigue tests were carried out at an elevated temperature, T_{right} of 329°C, stress ratio of $R = 0.05$, and frequency of 1 Hz. Fatigue performance of each fiber orientation was investigated at different maximum stress levels. The specimens that achieved the fatigue run-out condition of 2×10^5 cycles were subjected to tension-to-failure test in displacement control at a rate of 0.025 mm/s at elevated temperature in order to characterize the retained tensile properties.

The fatigue test procedure was developed using the MTS software. The temperature was initially ramped at a rate of 10°C/min to the set point obtained during

temperature calibration and kept constant for 45 min prior to loading. Then the specimen was subjected to cyclic loading with a sine waveform in force control until specimen failure or run-out were achieved. A specimen that achieved run-out of $2x10^5$ cycles was loaded in tension-to-failure to assess the retained tensile proprieties. The test procedure and data acquisition scheme used in this research were similar to those employed by Wilkinson [3] in prior work.

4.4 Optical Microscopy

In order to elucidate typical failure mechanisms, all tested specimens were examined with a Zeiss Discovery V12 stereoscopic optical microscope equipped with a Zeiss AxioCam HRc digital camera (see Figure 10).

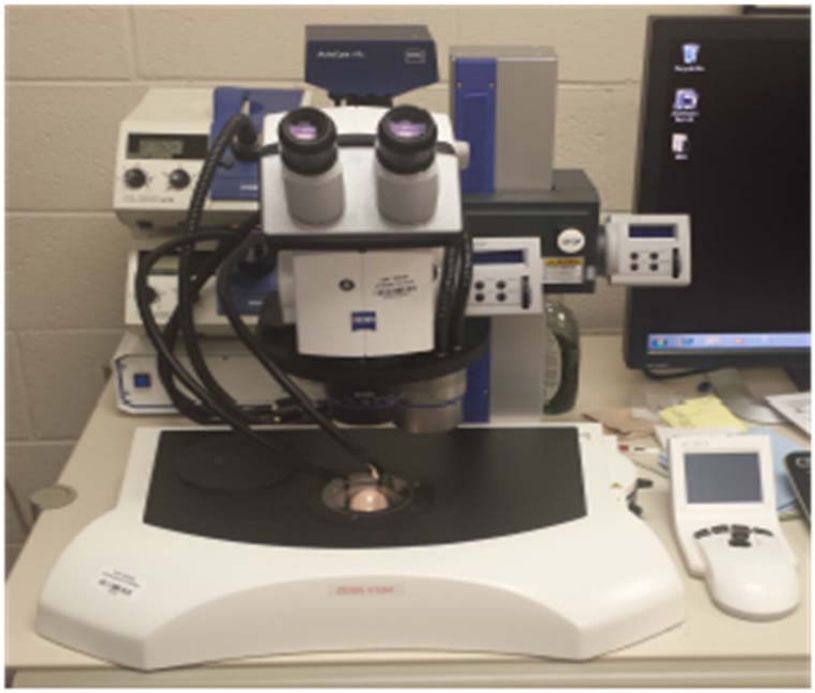

Figure 10. Zeiss optical microscope.

V. Results and Discussions

5.1 Assessment of Specimen-to-Specimen Variability

In this work, one panel of the unitized composite system was cut into 0/90 specimens while the other panel was cut into ±45° specimens. Notably, slight surface defects and thickness variations were observed among the specimens cut from the same panel. The surface defects and thickness variations are attributed to the composite manufacturing process. Results of the room-temperature modulus tests were used to assess specimen-to-specimen variability. The average room-temperature modulus values are presented in Table 9.

Table 9. Room-temperature elastic modulus.

	Specimen Type	Average Modulus (GPa)	Standard Deviation (GPa)	Coeff. Of Variation
MS4-1	T7: [0/90]	44.1139	5.3809	0.1219
MS4-2	T8: [±45]	13.2958	1.0447	0.0785

As expected, the modulus of the 0/90 specimens was greater than that of the ±45° specimens. However, 0/90 modulus values also exhibited greater variability. Distribution of 0/90 and ±45 modulus values is shown in Figure 11. We note that the 0/90 specimens had considerably more observable surface defects and greater thickness variations than the ±45 specimens. The presence of numerous surface defects and variations in thickness are likely behind the variations in room-temperature modulus values obtained for the 0/90 specimens.

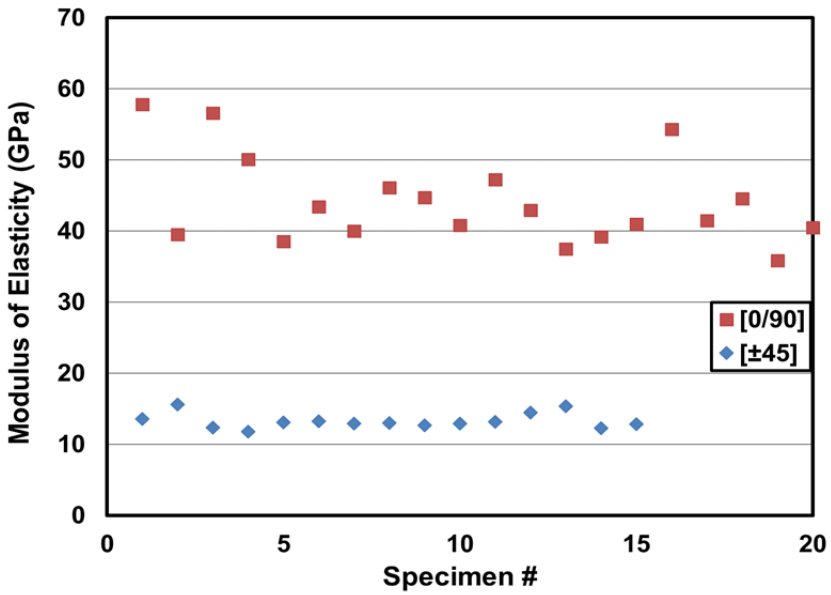

Figure 11. Distribution of room-temperature modulus values obtained for the unitized 2D PMC/3D CMC material system

The stresses obtained in tension-to-failure and tension-tension fatigue tests were normalized in order to facilitate comparison between data obtained for different specimens and for more consistent and relevant illustrations. Normalized stress was calculated using the following equation:

$$\sigma_{normalized} = \sigma_{actual} \frac{E_{avg}}{E_{specimen}} \tag{5.1}$$

Where $\sigma_{normalized}$ is the normalized stress value, σ_{actual} is the actual stress value, E_{avg} is the average modulus obtained for a given fiber orientation, and $E_{specimen}$ is the modulus of the individual specimen. The $\frac{E_{avg}}{E_{specimen}}$ is the normalization ratio for a given specimen. A specimen was considered to be stiffer (higher modulus) when the normalization ratio was less than one.

5.2 Thermal Expansion

All elevated temperature tests were performed with the right (CMC) side of the specimen at 329°C. The temperature was ramped to a set point at a rate of 10°C/min and then held constant for 45 min at zero load. The thermal strain was recorded during the temperature ramp up and dwell periods. A representative plot of the thermal stain is shown in Figure 12.

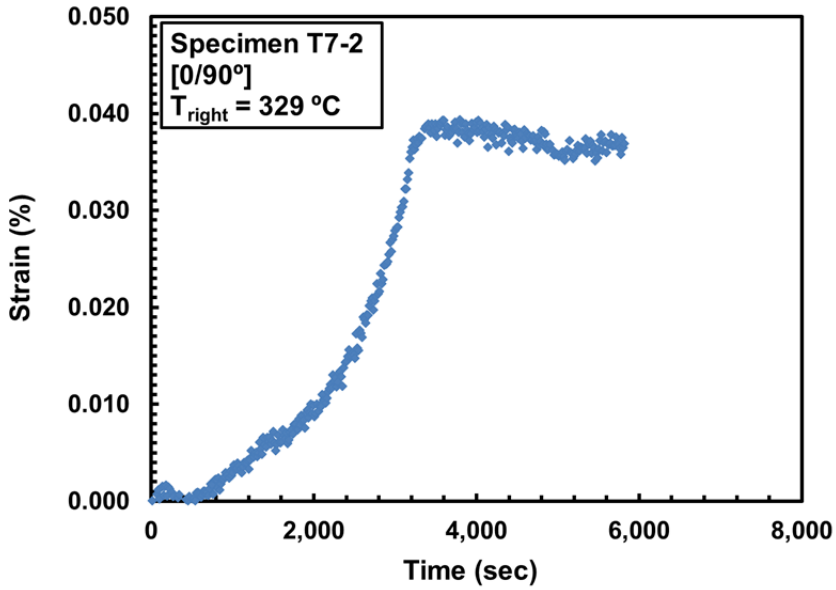

Figure 12. Thermal strain vs. time.

Variation in the T_{left} values noted in the course of this effort is attributed to variations in the laboratory ambient temperature. The thermal strains values obtained in this work are listed in Tables 10 and 11 for 0/90 and ±45 specimens, respectively.

Table 10. Thermal strain data obtained for 0/90 specimens

Fiber Orientation	Specimen #	T_{left} (°C)	T_{right} (°C)	Thermal Strain (%)
[0/90]	T7-1	65	329	0.037
	T7-2	67	329	0.037
	T7-4	64	329	0.038
	T7-6	65	329	0.043
	T7-7	68	329	0.012
	T7-8	70	329	0.020
	T7-9	67	329	0.023
	T7-10	74	329	0.028
	T7-12	64	329	0.021
	T7-13	67	329	0.040
	T7-14	72	329	0.008
	T7-15	68	329	0.019
	T7-17	70	329	0.034
	T7-19	69	329	0.046
	T7-20	67	329	0.008
	Average:	**67.8**	**329**	**0.028**

Table 11. Thermal strain data obtained for ±45° specimens

Fiber Orientation	Specimen #	T_{left} (°C)	T_{right} (°C)	Thermal Strain (%)
[±45]	T8-1	64	329	0.003
	T8-2	67	329	0.071
	T8-3	64	329	0.000
	T8-4	65	329	0.015
	T8-5	64	329	0.010
	T8-6	67	329	0.004
	T8-7	68	329	0.021
	T8-8	70	329	0.027
	T8-9	67	329	0.184
	T8-10	71	329	0.002
	T8-11	64	329	0.002
	T8-12	67	329	0.009
	T8-13	69	329	0.013
	T8-14	66	329	0.003
	T7-15	70	329	0.001
	Average:	**66.8**	**329**	**0.024**

It is instructive to compare the thermal strain values obtained in this work for the unitized 2D PMC/3D CMC material to those reported by Wilkinson [3] for the 2D PMC/2D CMC material system. We note that for each fiber orientation, the unitized 2D PMC/3D CMC material system produced smaller thermal strains than the 2D PMC/2D CMC material. The difference is particularly pronounced in the case of the ±45 specimens. It is likely that the 3D architecture offers more thermal protection in the case of the ±45 fiber orientation.

Table 12. Thermal strain data obtained for 2D PMC/2D CMC. Data from Wilkinson [3].

Material	Fiber Orientation	Thermal Strain (%)
MS3	[0/90]	**0.026**
	[±45]	**0.043**

5.3 Monotonic Tensile Tests at Elevated Temperature

5.3.1 Experimental Results.

Due to a limited number of test specimens investigating material properties and behavior under conditions simulating the intended operating conditions was deemed a priority. Hence the tensile-to-failure tests were conducted only at elevated temperature (T_{right} = 329°C). The test results are summarized in Tables 13 and 14. The failure was taken to occur when a dramatic instantaneous drop in stress took place.

Table 13. Summary of tensile properties for the 2D PMC/3D CMC with 0/90 fiber orientation at elevated temperature (T_{right} = 329°C)

Fiber Orientation	Specimen #	Temperature Left/Right (°C)	Elastic Modulus (GPa)	Normalized Modulus (GPa)	UTS (MPa)	Normalized UTS (MPa)	Failure Strain (%)
[0/90]	T7-10	74/329	41.80	41.04	479.19	470.50	0.992
	T7-15	68/329	38.17	37.30	513.15	501.73	1.726
	Average:	**71/329**	**39.98**	**39.17**	**496.17**	**486.11**	**1.359**

Table 14. Summary of tensile properties for the 2D PMC/3D CMC with ±45 fiber orientation at elevated temperature (T_{right} = 329°C)

Fiber Orientation	Specimen #	Temperature Left/Right (°C)	Elastic Modulus (GPa)	Normalized Modulus (GPa)	UTS (MPa)	Normalized UTS (MPa)	Failure Strain (%)
[±45]	T8-5	64/329	8.08	8.00	93.82	92.69	5.402
	T8-6	67/329	9.62	9.38	96.96	94.45	4.608
	Average:	**55.5/329**	**8.85**	**8.69**	**95.39**	**93.57**	**5.005**

For the 0/90° fiber orientation two specimens were tested in tension to failure at elevated temperature. Results in Table 13 reveal that the temperature of the left side of the specimen (i. e. the side open to ambient air) was fluctuating from test to test. The average ultimate tensile strength (UTS) was 496.17 MPa, the average modulus was 39.98 GPa, and the average failure strain was 1.36%. Figure 13 shows the tensile stress-strain curves for the 0/90° fiber orientation.

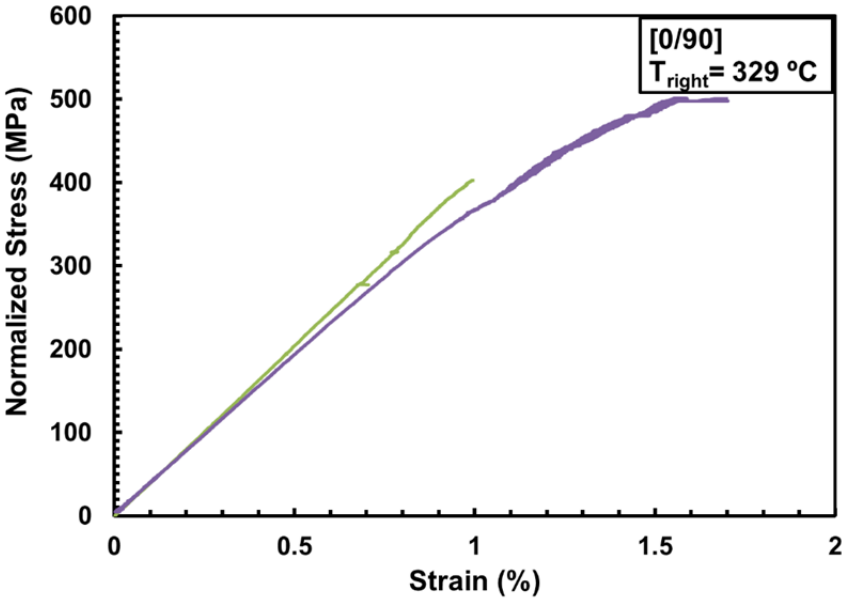

Figure 13. Tensile stress-strain curves obtained for the 2D PMC/3D CMC with 0/90 fiber orientation at elevated temperature.

Likewise, two specimens with ±45° fiber orientation were tested in tension to failure at elevated temperature. Figure 14 shows the corresponding stress-strain curves. The average UTS was 95.39 MPa, the average modulus was 8.85 GPa, and the average failure strain was ~5.0%. The tensile stress-strain curves obtained for the 0/90° and ±45° fiber orientations are plotted together in the Figure 15. It is seen that the ±45 tensile strength is much lower than the 0/90 tensile strength. In fact, the ±45° UTS was only 19% of the 0/90° UTS. This result was expected since the matrix material bears the majority of the load for off-axis specimens. Furthermore, a complete failure of the ±45 specimens did not occur when the stress reached the UTS value. Actually, the strain continuous to accumulate with some fibers were still resisting the load.

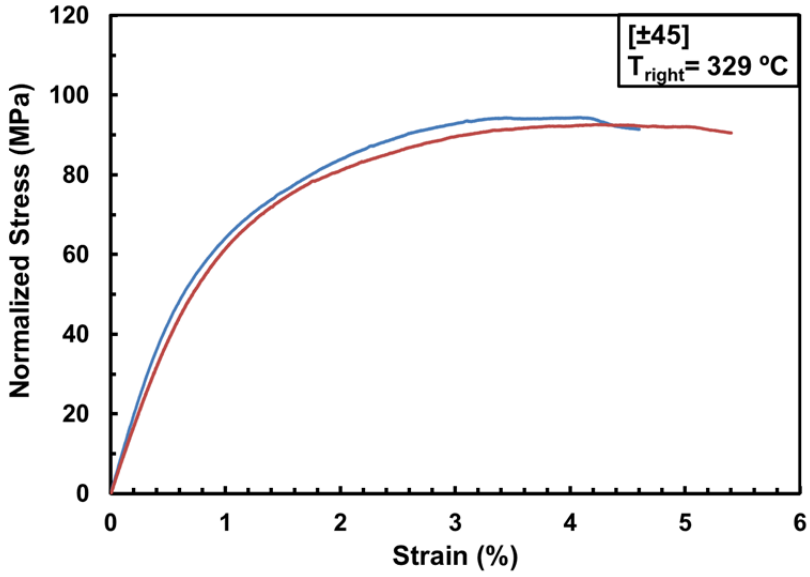

Figure 14. Tensile stress-strain curves obtained for the 2D PMC/3D CMC with ±45° fiber orientation at elevated temperature.

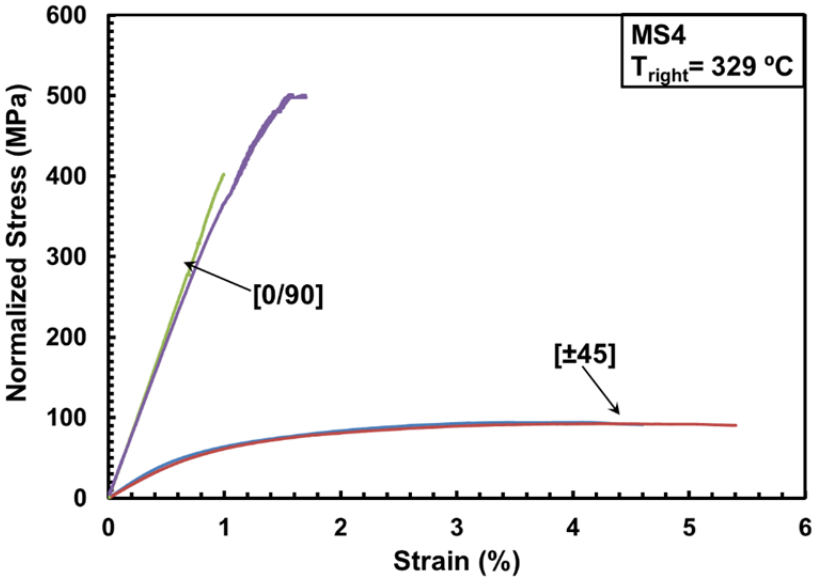

Figure 15. Tensile stress-strain curves obtained for the 2D PMC/3D CMC with 0/90° and ±45° fiber orientations at elevated temperature.

5.3.2 Comparison of Tensile Properties Obtained for the 2D PMC/3D CMC with the Tensile Properties Obtained for the 2D PMC and the 2D PMC/2D CMC at Elevated Temperature.

The stress-strain response obtained in monotonic tension for the 2D PMC/3D CMC (MS4) is compared with the stress-strain results obtained for the 2D PMC (MS2) and the 2D PMC/2D CMC (MS3) by Wilkinson [3]. The results are summarized in Table 15. Figure 16 contrasts the tensile stress-strain curves obtained for the 2D PMC/3D CMC (MS4), 2D PMC (MS2), and 2D PMC/2D CMC (MS3) with 0/90° fiber orientation. In contrary to both material systems previously evaluated which showed similar average stiffness and similar average failure strains, the MS4 presented much lower UTS and higher failure strain. There is a decrease in elasticity modulus. It is most likely that additional loads interacted due to the complex nature of material that it is formed by different components and caused the loss in strength.

Table 15. Summary of tensile properties for the 2D PMC (MS2) and the 2D PMC/2D CMC (MS3) at elevated temperature (T_{right} = 329°C). Data from Wilkinson [3].

Material	Fiber Orientation	Normalized Modulus (GPa)	Normalized UTS (GPa)	Failure Strain (%)
MS2	[0/90]	**59.95**	**821.5**	**1.281**
	[±45]	**13.48**	**128.3**	**12.955**
MS3	[0/90]	**57.85**	**664.2**	**1.200**
	[±45]	**9.22**	**56.35**	**2.539**

Failure strain is based on 50% load drop.

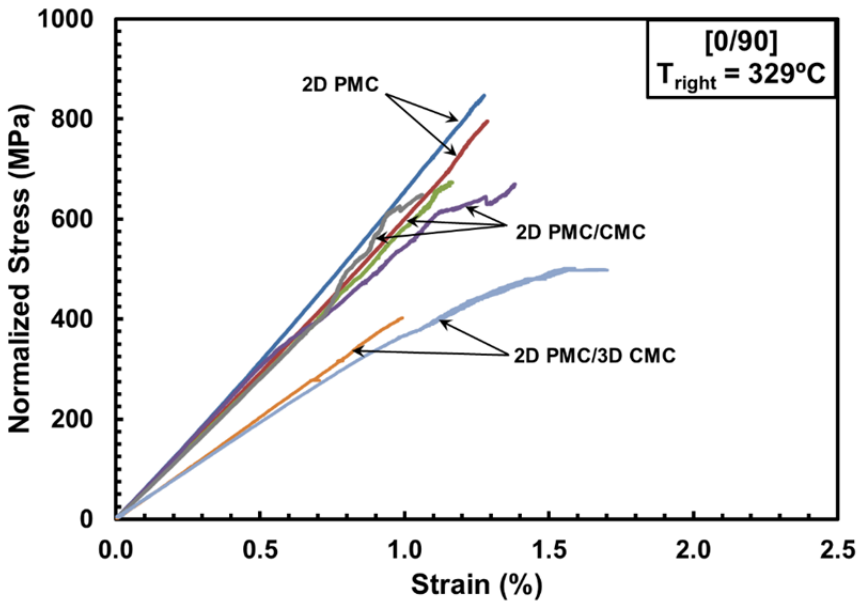

Figure 16. Tensile stress-strain curves obtained for the MS2, MS3, and MS4 with 0/90° fiber orientation at elevated temperature. MS2 and MS3 results from Wilkinson [3].

In a similar manner, Figure 17 contrasts the tensile stress-strain curves obtained for the three material systems with ±45° fiber orientation. Although the MS2 (2D PMC) with ±45 fiber orientation exhibited higher strength, stiffness, and failure strain than the MS4 with the ±45° fiber orientation at elevated temperature, the MS4 showed better tensile properties than the MS3 (2D PMC/2DCMC) with higher UTS and failure strain, and only slightly lower modulus.

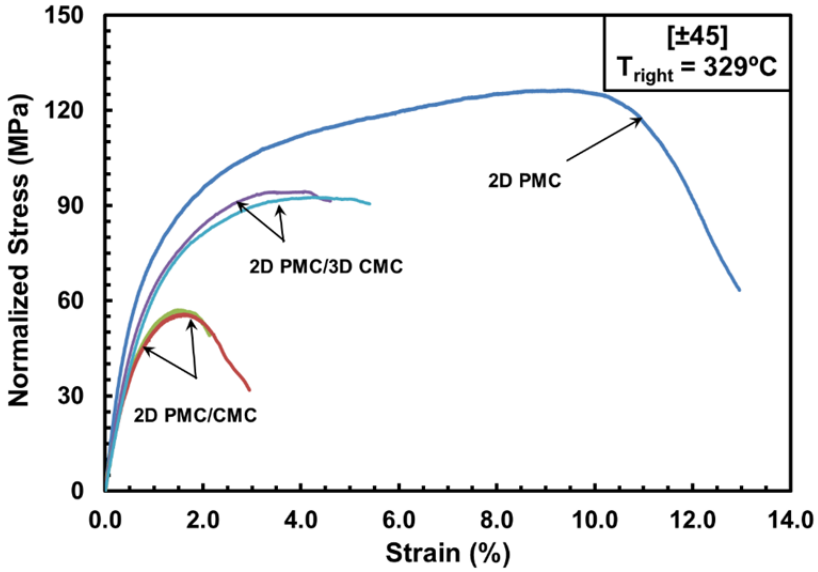

Figure 17. Tensile stress-strain curves obtained for the MS2, MS3, and MS4 with ±45° fiber orientation at elevated temperature. MS2 and MS3 results from Wilkinson [3].

In summary, the comparison of tensile behavior and properties produced by different material systems at elevated temperature demonstrated that the MS4 (2D PMC/3D CMC) exhibited lower UTS and lower modulus than both the MS2 (2D PMC) and the MS3 (2D PMC/2D CMC) with the 0/90° fiber orientation. The failure strain was nearly the same for the three composites. For the ±45° fiber orientation, the MS2 exhibited higher strength and stiffness, and a significantly greater failure strain than both unitized composites. Conversely, the MS4 showed higher UTS, slightly lower modulus and greater failure strain than the MS3.

5.4 Tension-Tension Fatigue at Elevated Temperature

All fatigue tests were conducted at an elevated temperature, T_{right}, of 329°C with a minimum to maximum stress ratio of R = 0.05 at a frequency of 1 Hz. Fatigue run-out was set to $2x10^5$ cycles. This section will discuss the fatigue results for the MS4 and compare it to fatigue performance of the MS2, and the MS3.

5.4.1 Fatigue Performance of Material System 4 (2D PMC/3D CMC).

Fatigue results for the MS4 specimens are summarized in Tables 16 and 17. A significant variability was seen in the number of cycles sustained in tests performed with some of the lower and intermediate stress levels. For example, T7-13 tested with σ_{max} of 82%UTS sustained 542 cycles, whereas specimen T7-1 tested with σ_{max} of 83%UTS achieved a run-out. The early failures are attributed to severe ply delamination observed for these specimens.

The maximum stress vs. cycles to failure (S-N) curve for the 0/90° orientation is shown in the Figure 18. The S-N curve for the ±45° fiber orientation is presented in Figure 19. Note that the S-N curve obtained for the 0/90 fiber orientation is nearly flat. Furthermore, in case of the 0/90 fiber orientation the fatigue limit is at 85% UTS. Contrastingly, in the case of the ±45 fiber orientation, the fatigue limit is only at 45% UTS.

Table 16. Tension-tension fatigue results for MS4 with 0/90° fiber orientation at T_{right} = 329°C in laboratory air.

Fiber Orientation	Specimen #	Maximum Stress (MPa)	Maximum Stress (% UTS)	Normalized Max Stress (MPa)	Normalized Max Stress (% Norm UTS)	Cycles to Failure (N)	Failure Strain (%)
[0/90]	T7-7	300	60	331	62	200,000[a]	1.811[a]
	T7-14	370	75	417	78	200,000[a]	2.549[a]
	T7-1	410	83	313	58	200,000[a]	5.984[a]
	T7-8	420	85	402	75	200,000[a]	---
	T7-19	400	81	492	92	84,203	4.075
	T7-20	420	85	458	86	56,566	1.861
	T7-17	400	81	426	80	33,208	1.524
	T7-6	435	88	442	82	32,893	3.872
	T7-4	430	87	335	63	10,326	2.165
	T7-13	405	82	476	89	542	2.353
	T7-2	450	91	502	94	317	2.364
	T7-9	430	87	424	79	308	2.231
	T7-12	450	91	462	86	32	1.474

[a] Run-out; defined as $2x10^5$ cycles. Failure of specimen did not occur when the test was terminated.

Table 17. Tension-tension fatigue results for MS4 with ±45° fiber orientation at T_{right} = 329°C in laboratory air

Fiber Orientation	Specimen #	Maximum Stress (MPa)	Maximum Stress (% UTS)	Normalized Max Stress (MPa)	Normalized Max Stress (% Norm UTS)	Cycles to Failure (N)	Failure Strain (%)
[±45]	T8-9	38	40	40	41	200,000[a]	0.903[a]
	T8-10	43	45	44	46	200,000[a]	0.475[a]
	T8-14	52	55	56	58	99,013	3.768
	T8-11	48	50	49	50	48,384	4.014
	T8-15	57	60	59	61	45,035	---
	T8-8	48	50	49	51	44,533	1.951
	T8-7	57	60	62	64	39,061	2.151
	T8-13	62	65	54	56	16,890	---
	T8-2	72	75	61	64	4,756	1.985
	T8-12	67	70	62	64	2,155	5.899
	T8-1	76	80	75	77	1,070	6.558
	T8-3	67	70	72	75	298	2.535
	T8-4	67	70	75	78	276	2.703

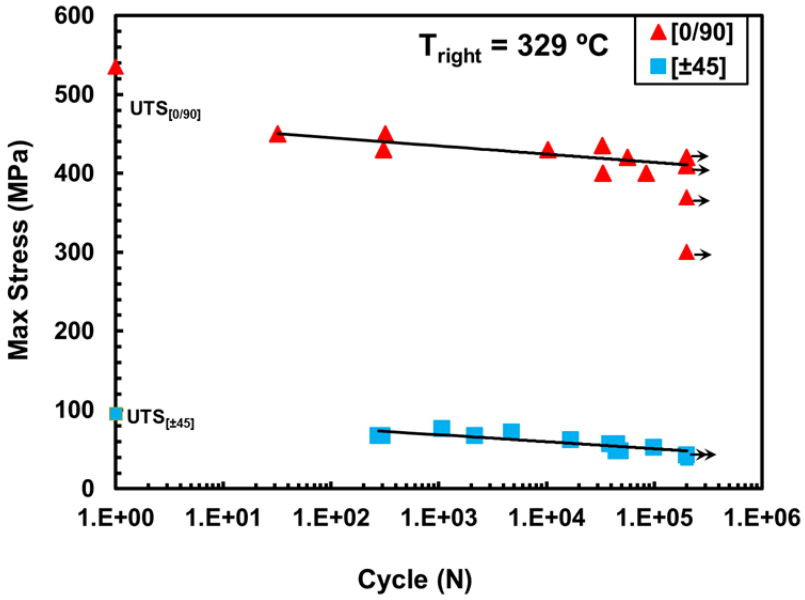

Figure 18. S -N curves for the MS4 at elevated temperature. Arrow indicates specimen achieved fatigue run-out.

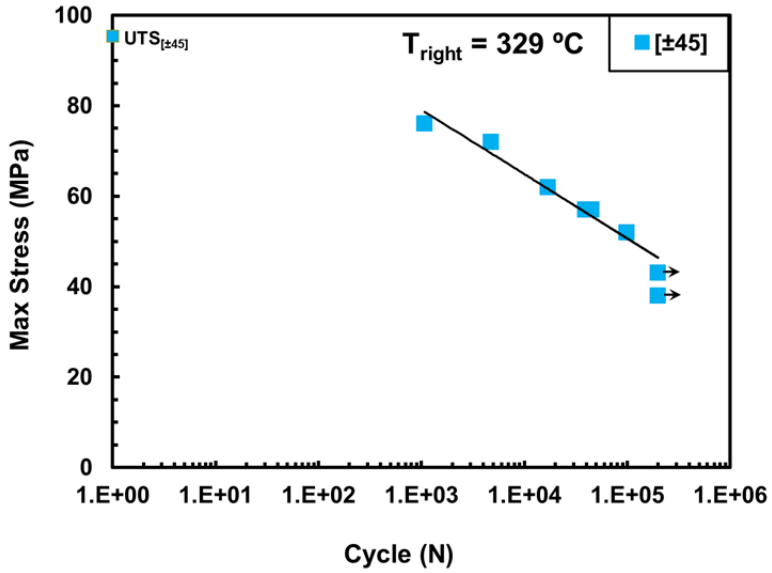

Figure 19. S -N curves for the MS4 with ±45° fiber orientation at elevated temperature. Arrow indicates specimen achieved fatigue run-out.

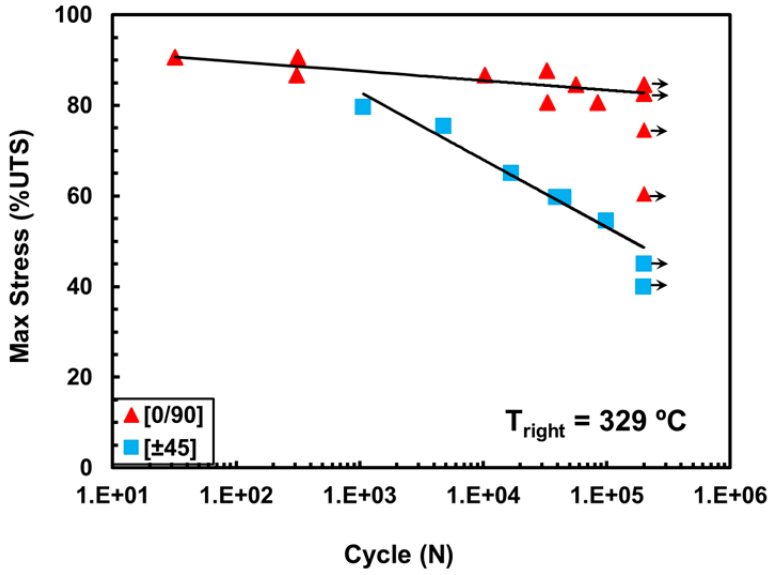

Figure 20. S -N curves for the MS4 at elevated temperature. Maximum stress is shown as % UTS. Arrow indicates specimen achieved fatigue run-out.

Figure 21 displays the evolution of stress-strain hysteresis response with fatigue cycles of an MS4 specimen with 0/90° fiber orientation that achieved run-out for a maximum fatigue stress of 410 MPa (83% UTS). During the first cycle, the response is almost linear elastic. As the test progresses, the strain starts to accumulate with more damage occurring, and the hysteresis stress-strain loops begin to open up and acquire a slight "S" shape. The slope of the stress-strain loop first decreases and then increases. This phenomenon can be attributed to the extensive delamination occurring in the specimen gage section. Additionally, it is recognized that the unitized composite that consists of two dissimilar materials co-cured together will exhibit non-homogeneous deformation in the specimen gage section.

The stress-strain plot obtained for T7-9 specimen is shown in Figure 22. This specimen was fatigued with a maximum stress of 430 MPa (87%UTS). Ply delamination

was observed early in this test. As the cycling continues, the stiffness decreases and appreciable strain is accumulated.

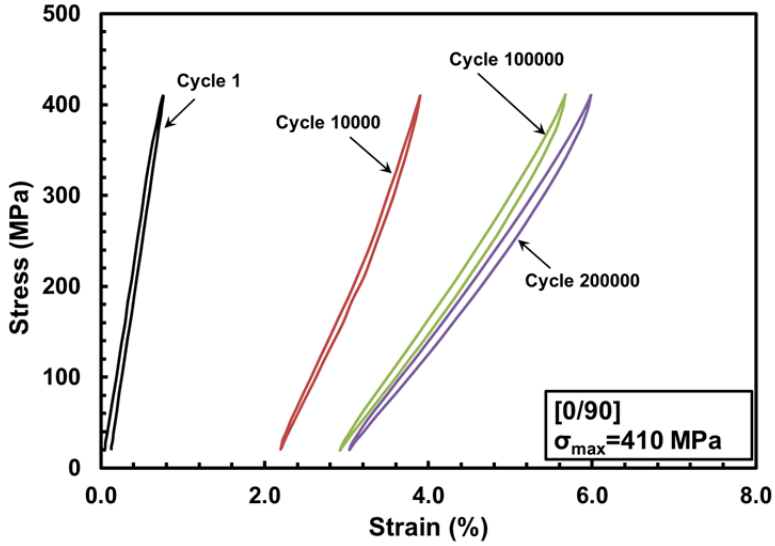

Figure 21. Evolution of stress-strain hysteresis response with fatigue cycles for specimen T7-1 of the MS4 with 0/90° fiber orientation at elevated temperature.

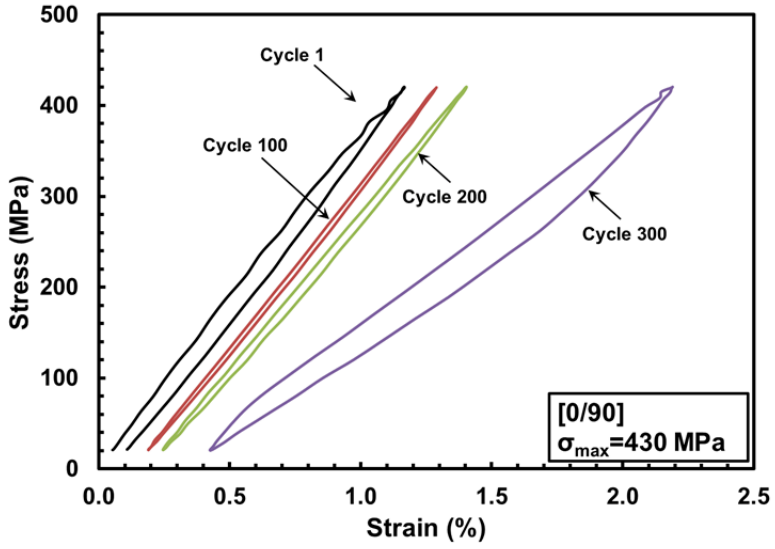

Figure 22. Evolution of stress-strain hysteresis response with fatigue cycles for specimen T7-9 of the MS4 with 0/90° fiber orientation at elevated temperature.

Reduction in stiffness (hysteresis modulus determined from the maximum and minimum stress-strain data points during a load cycle) during cycling for the MS4 specimens with 0/90° fiber orientation can be seen in Figure 23. Considering the initial severe delamination and appreciable strain accumulated during the first cycle, the modulus was normalized to the modulus of the second cycle rather than to the modulus of the first cycle. Early in the fatigue test the modulus remains nearly constant then starts to decrease steadily until failure. The amount of modulus loss varied between 20% and 75%. The specimens that achieved run-out produced the highest modulus loss. This was expected since the damage in the material was accumulating consistently as the cycling progressed.

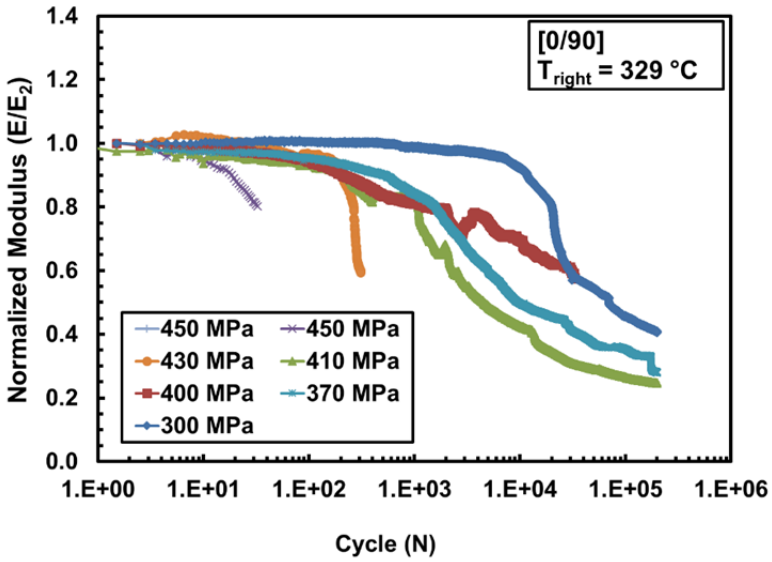

Figure 23. Normalized modulus vs. fatigue cycles for the MS4 with 0/90° fiber orientation at elevated temperature.

Maximum and minimum strains vs. fatigue cycles for the 0/90° specimens are shown in Figure 24. The minimum strain which is the strain accumulated during cycling ranged from 0.2% to 0.5%.

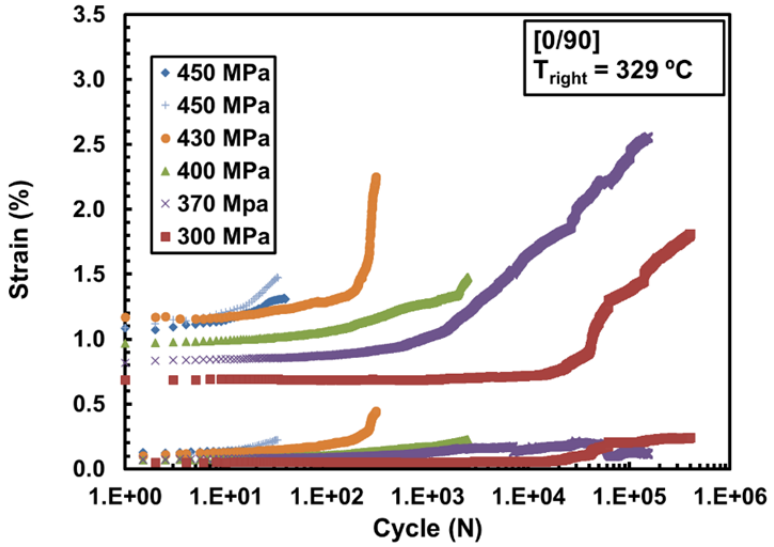

Figure 24. Maximum and minimum strains vs. fatigue cycles for the MS4 with 0/90° fiber orientation at elevated temperature.

The evolution of stress-strain hysteresis response with fatigue cycles obtained for an MS4 specimen with ±45 fiber orientation tested with fatigue stress of 57 MPa (60% UTS) can be seen in Figure 25. The stress-strain response reveals the viscoelastic behavior of the material as the loops are not linear. Note that the hysteresis modulus decreases as the specimen approaches failure.

Normalized hysteresis modulus vs. fatigue cycles is presented in Figure 26. In tests performed with lower fatigue stresses the modulus initially increases slightly then decreased as the cycling continues. This initial increase in modulus is attributed to the fibers realigning in the direction of applied load (fiber tow "scissoring"). In tests

performed with intermediate and higher fatigue stresses the modulus decreases steadily and drops dramatically as the specimen approaches failure. The amount of modulus loss ranged from 2% to 70%.

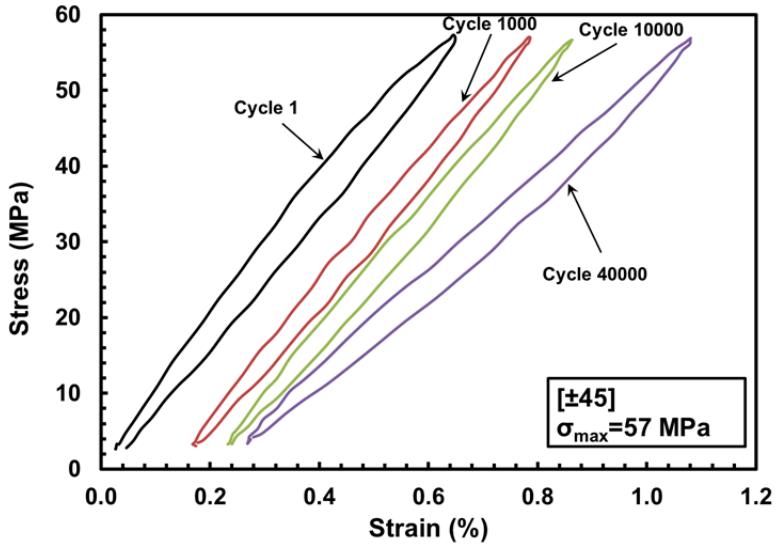

Figure 25. Evolution of stress-strain hysteresis response with fatigue cycles for specimen T8-15 of the MS4 with ±45° fiber orientation at elevated temperature.

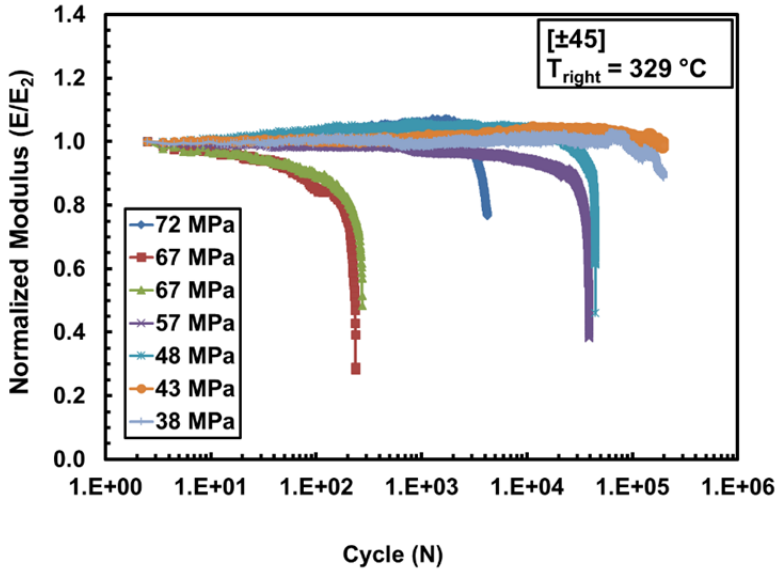

Figure 26. Normalized modulus vs. fatigue cycles for the MS4 with ±45° fiber orientation at elevated temperature.

Maximum and minimum strains vs. fatigue cycles for the ±45° specimens are seen in Figure 27. Note significant strain ratcheting. Strains accumulated during cycling from 0.054% to 1.306%.

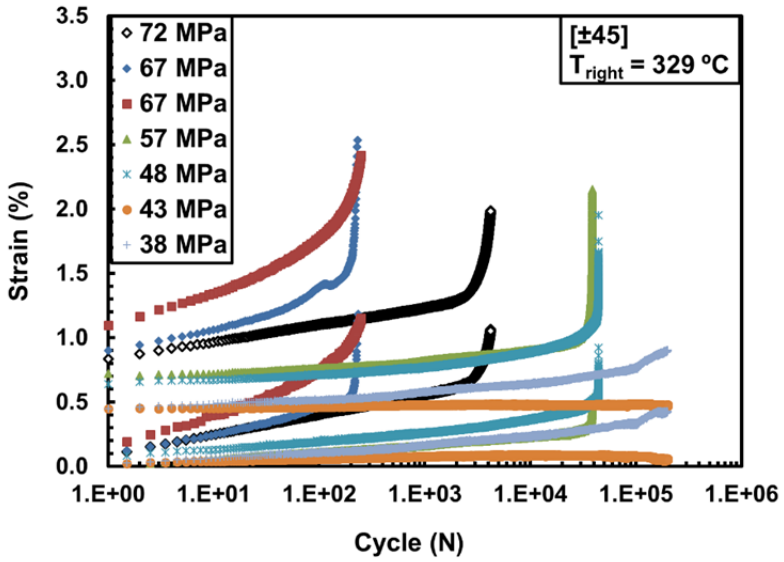

Figure 27. Maximum and minimum strains vs. fatigue cycles for the MS4 with ±45° fiber orientation at elevated temperature.

5.4.2 Comparison of Fatigue Performance of MS4 to MS2 and MS3 Composites.

The fatigue performance of the MS4 with 0/90° fiber orientation is compared to the fatigue performance of the MS2 (2D PMC) and MS3 (2D PMC/2D CMC) in Figure 28. The S-N curves for the MS3 and MS2 occur at greater stress levels than the S-N curve for the MS4. Notably the MS4 produced the lowest fatigue limit. The MS4 fatigue limit is 73% of the MS2 fatigue limit and 89% of the MS3 fatigue limit.

Fatigue S-N results obtained for the three composites with 0/90 fiber orientation are also compared in Figures 29 and 30 where stress is shown in % UTS. It is seen that MS4 fatigue limit lies at greater percentage of the corresponding UTS than the MS2 and MS3 fatigue limits.

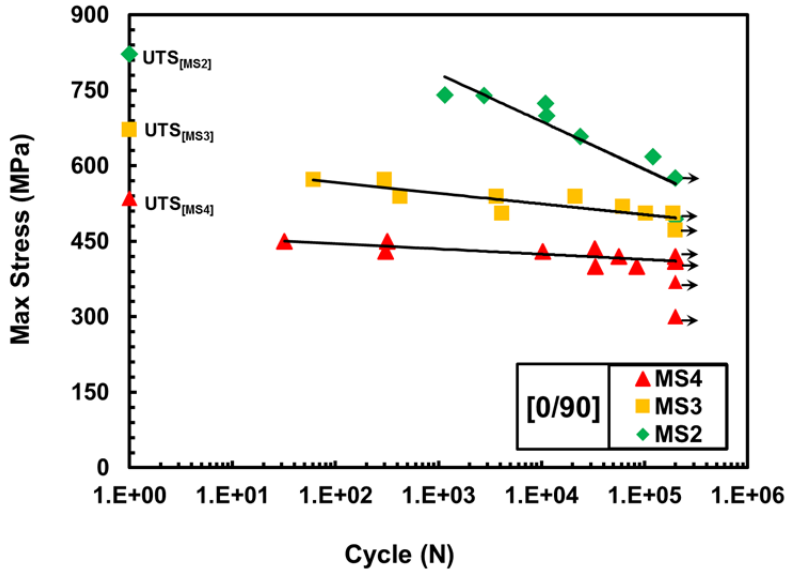

Figure 28. S-N curves for the MS4, MS3, and MS2 with 0/90° fiber orientation at elevated temperature. Arrow indicates specimen achieved fatigue run-out. MS2 and MS3 data from Wilkinson [3].

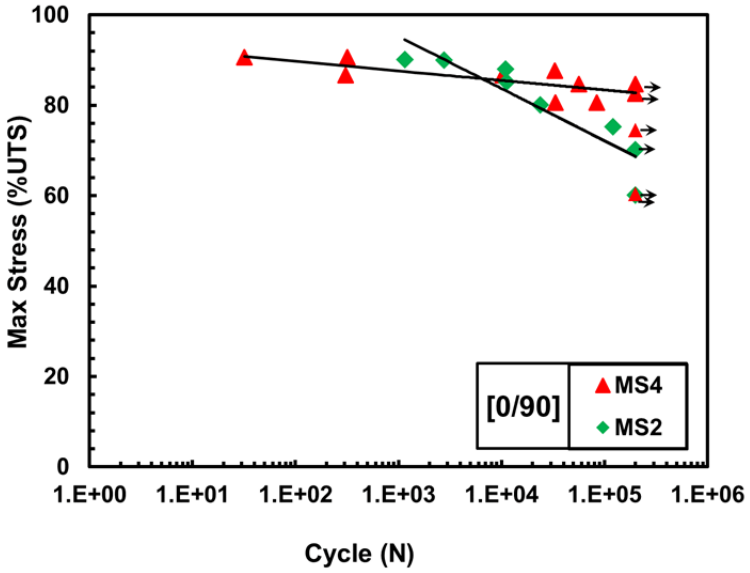

Figure 29. S-N curves for the MS4 and MS2 with 0/90° fiber orientation at elevated temperature. Maximum stress is shown as % UTS. Arrow indicates specimen achieved fatigue run-out. Maximum stress is shown as % UTS. MS2 and MS3 data from Wilkinson [3].

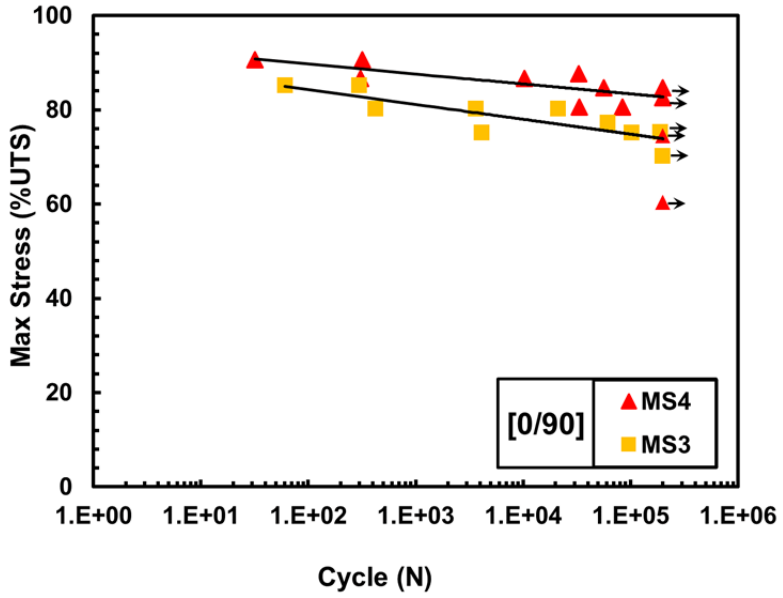

Figure 30. S-N curves for the MS4 and MS3 with 0/90° fiber orientation at elevated temperature. Maximum stress is shown as % UTS. Arrow indicates specimen achieved fatigue run-out. Maximum stress is shown as % UTS. MS2 and MS3 data from Wilkinson [3].

Fatigue performance of the three material systems with ±45° fiber orientation is compared in Figure 31. It is seen that the MS2 offers better tension-tension fatigue than the unitized composites. The fatigue limit obtained for the MS2 is some 38% higher than that obtained for the MS4. Conversely, when we examine S-N curves in Figures 32 and 33 where maximum stress is shown as %UTS, the three material systems display relatively similar fatigue performance.

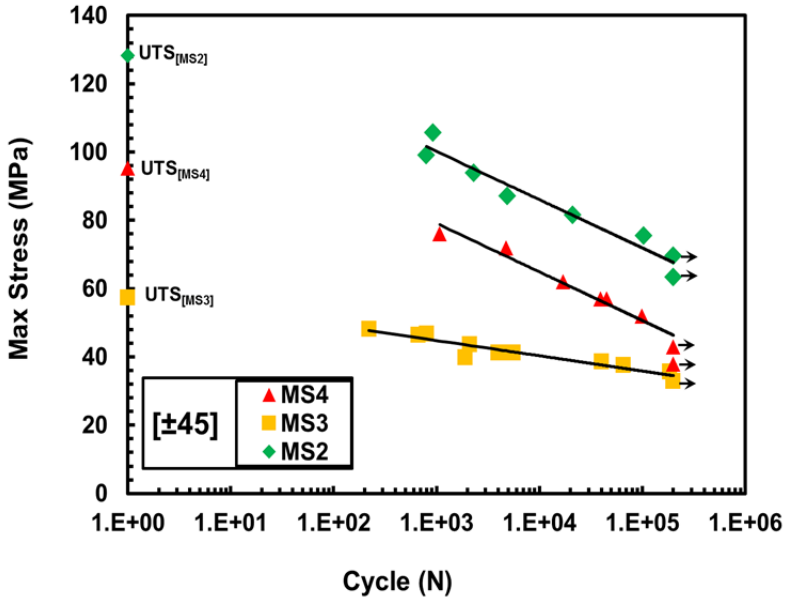

Figure 31. S-N curves for the MS4, MS3, and MS2 with ±45° fiber orientation at elevated temperature. Arrow indicates specimen achieved fatigue run-out. MS2 and MS3 data from Wilkinson [3].

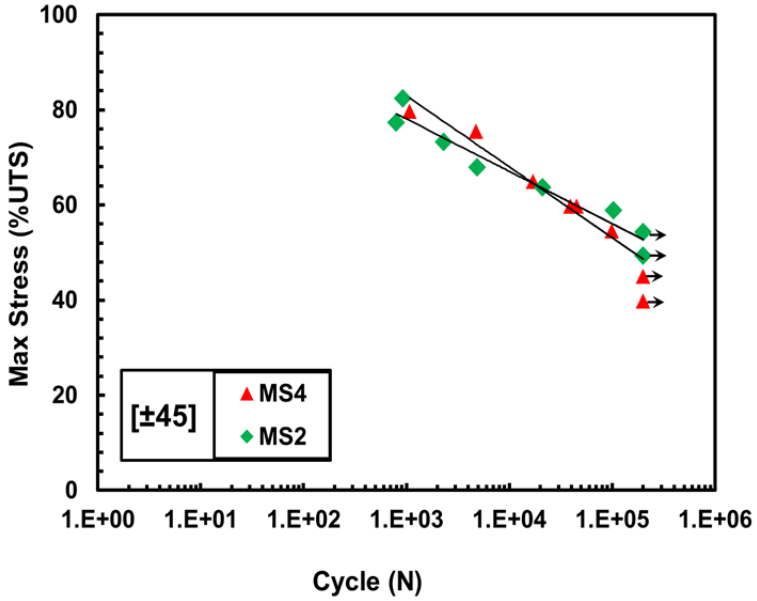

Figure 32. S-N curves for the MS4 and MS2 with ±45° fiber orientation at elevated temperature. Maximum stress is shown as % UTS. Arrow indicates specimen achieved fatigue run-out.

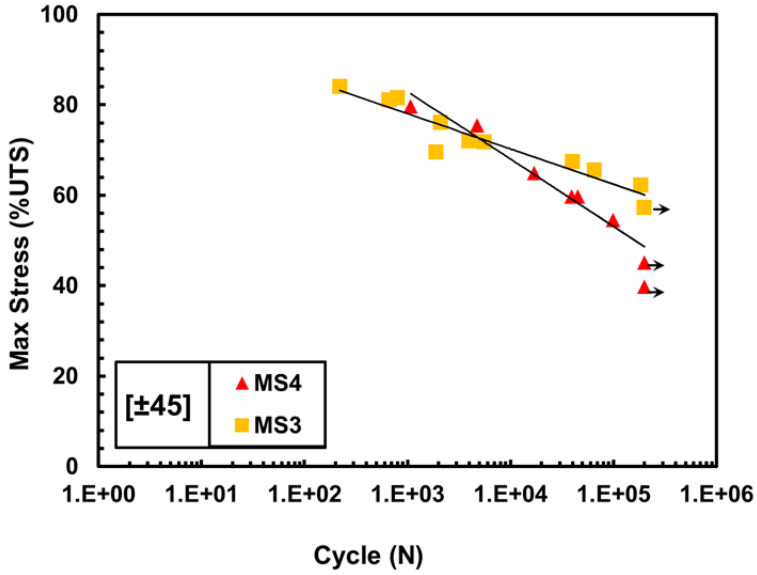

Figure 33. S-N curves for the MS4 and MS3 with ±45° fiber orientation at elevated temperature. Maximum stress is shown as % UTS. Arrow indicates specimen achieved fatigue run-out.

5.5 Post-Fatigue Retained Tensile Properties

All specimens that achieved fatigue run-out were subjected to tension-to-failure test at elevated temperature (T_{right} =329°C) in order to measure the retained tensile properties. The retained tensile properties are summarized in Table 18 and Figure 34.

The retained tensile stress-strain curve for the MS4 with 0/90° fiber orientation is shown in Figure 35 along with the stress-strain curve for the as-processed material. It is clearly seen that prior fatigue especially with high fatigue stress levels causes significant loss in stiffness. The average stiffness loss was 37.5%. Conversely, the loss of tensile strength was minimal. On the average, the 0/90 specimens retained 93% of their tensile strength.

Table 18. Retained tensile properties of the MS4 specimens subjected to prior fatigue at T_{right}= 329°C in laboratory air

Fiber Orientation	Specimen #	Fatigue Stress (MPa)	Retained Modulus (GPa)	Modulus Retention (%)	Retained Strength (MPa)	Strength Retention (%)	Failure Strain (%)
[0/90]	T7-07	300	33.34	83.6	480.0	96.7	2.888
	T7-14	370	14.85	37.1	426.3	85.9	3.261
	T7-01	410	16.19	40.5	490.6	98.8	3.645
	T7-08	420	35.38	88.5	448.0	90.3	---
[±45]	T8-09	38	7.72	87.1	71.66	75.1	6.411
	T8-10	43	9.84	111.1	92.48	96.9	4.123

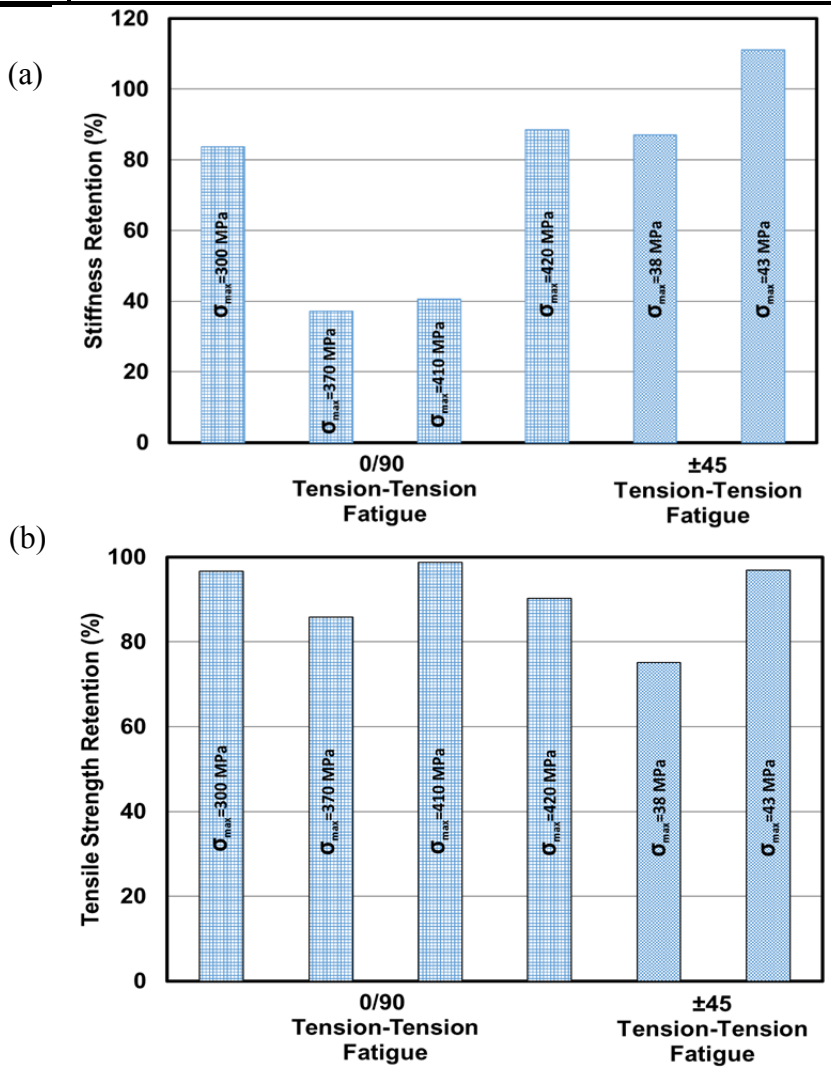

Figure 34. Retention of (a) stiffness and (b) tensile strength of the MS4 specimens subjected to prior fatigue at T_{right}= 329°C in laboratory air

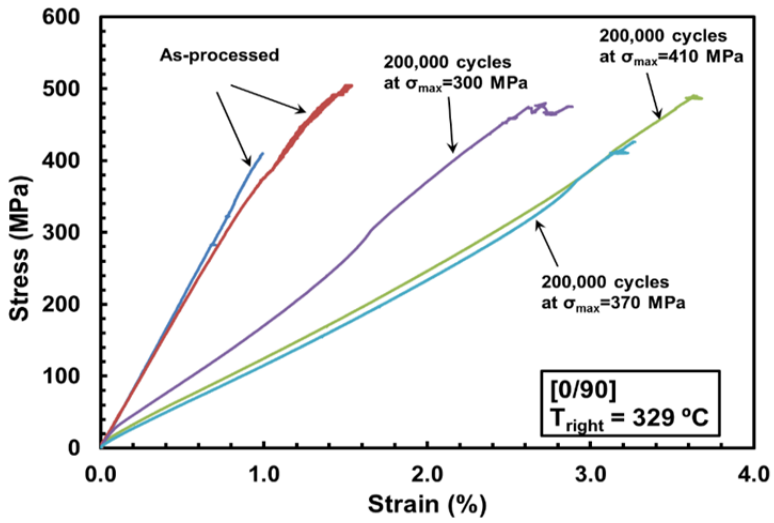

Figure 35. Stress vs. strain for the MS4 with 0/90° fiber orientation subjected to prior fatigue at elevated temperature. Stress-strain curves for the as-processed material are shown for comparison.

The tensile stress-strain curves obtained for the MS4 ±45° specimens subjected to prior fatigue are plotted in Figure 36 together with the stress-strain curves for the as-processed material. For the specimen pre-fatigued at 43 MPa, the stiffness increased by 11% and the strength dropped by 3%. For the specimen subjected to prior fatigue at 38 MPa, the modulus and strength decreased by 13% and 25%, respectively.

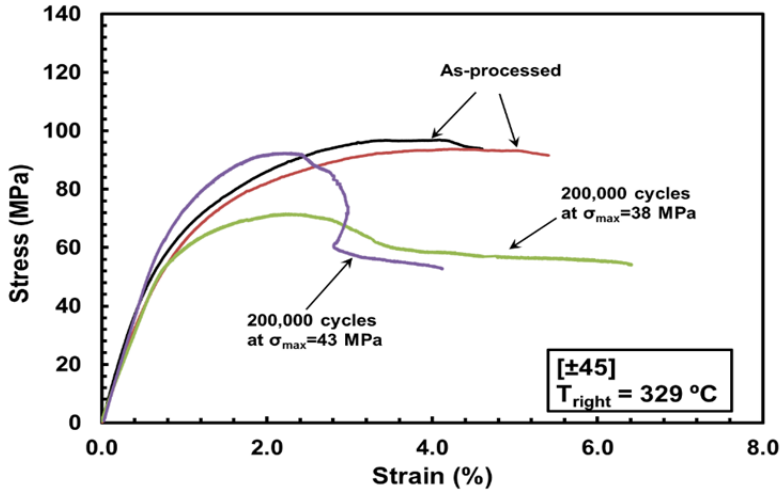

Figure 36. Stress vs. strain for the MS4 with ±45° fiber orientation subjected to prior fatigue at elevated temperature. Stress-strain curves for the as-processed material are shown for comparison.

Additionally, for each specimen that achieved fatigue run-out the retained modulus can be compared to the elastic modulus obtained during the 1st cycle of the fatigue test. The purpose of such comparison is to evaluate the effect of the loading rate on the modulus. Recall that the tension-to-failure test is performed at a displacement rate of 0.025 mm/s, while in the fatigue cycle the increase from minimum to maximum load occurs in 0.5 s. Results are given in the Table 19. No significant differences are noted between the retention modulus percentages calculated using as-processed tension-to-failure moduli and those calculated using the first cycle load-up modulus. This observation holds for both fiber orientations. We conclude that the loading rate has little to no effect on the modulus.

Table 19. Retained properties of the MS4 specimens subjected to prior fatigue at T_{right}= 329°C in laboratory air

Fiber Orientation	Specimen #	Fatigue Stress (MPa)	Retained Modulus (GPa)	1st Cycle Modulus (GPa)	1st Cycle Modulus Retention (%)
[0/90]	T7-07	300	33.34	41.12	81.0
	T7-14	370	14.85	46.58	31.8
	T7-01	410	16.19	47.52	34.0
	T7-08	420	35.38	37.80	93.5
[±45]	T8-09	38	7.72	9.54	80.9
	T8-10	43	9.84	11.08	88.8

5.6 Optical Microscopy Examination

As-processed specimens, one for each fiber orientation, as well as specimens tested in either tension-to-failure or tension-tension fatigue were examined under the Zeiss optical microscope. The optical micrographs were used to study the damage and failure mechanism in the unitized composite MS4.

5.6.1 Examination of the MS4 specimens with 0/90 fiber orientation.

Figure 37 shows different views of the gage section of as-processed MS4 specimen with 0/90˚ fiber orientation. The optical micrographs reveal the rugged texture of the CMC portion. Notably, specimen thickness was uneven. Additionally, numerous matrix voids and pits were observed in the PMC portion.

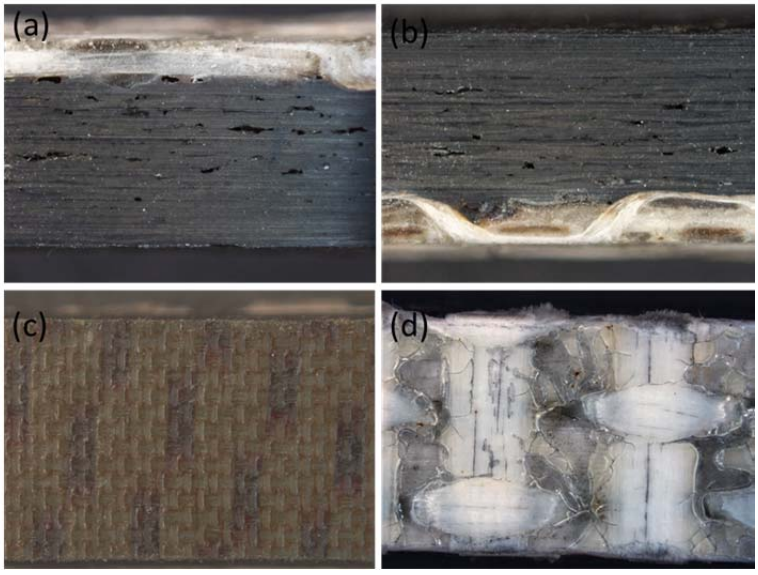

Figure 37. Optical micrographs of as-processed MS4 specimen with 0/90° fiber orientation (T7-2): (a)-(b) side views, (c) PMC face, (d) CMC face.

Figure 38 shows stitched optical micrographs of two 0/90° specimens that achieved fatigue run-out and were subsequently failed in tension test. Specimen T7-8 was tested in fatigue with the maximum stress of 420 MPa, while specimen T7-1 was tested in fatigue with maximum stress of 410 MPa. These specimens were intentionally not broken in two parts after failure in order to image the non-homogeneous deformation in the gage section. Delamination is evident as is slight bowing out of the composite plies. Because the unitized composite consists of two dissimilar materials co-cured together,

deformation in the specimen gage section is non-homogeneous. It is likely that this non-homogeneous deformation causes bending stresses in addition to the applied tensile stress. Also note the cracks propagating through the PMC part that often extend from the gage section into the gripping sections of the specimen.

Similar non-homogeneous deformation and bowing out of composite plies were reported for the MS3 (2D PMC/2D CMC) 0/90 specimens subjected to tensile loads (see Figure 39). Note that the bowing out of plies is much more pronounced in the case of MS3 than for MS4. Recall that the CMC portion of MS3 consists of three 2D plies and shows severe delamination. In contrast, the CMC portion of MS4 consists of a single 3D ply which resists delamination. Hence bowing out of the 3D CMC ply is minimal.

Notably the non-homogeneous deformation and bowing out of plies were also observed during tension-tension fatigue cycling. The plies bow out during loading and return to original shape during unloading (see schematic in Figure 40).

Figure 38. Stitched optical micrographs of the MS4 0/90° specimens T7-8 and T7-1 after failure in tension at elevated temperature.

Figure 39. Stitched optical micrographs of MS3 0/90° specimen T5-2 following failure in tension at room temperature and load removal. From Wilkinson [3]

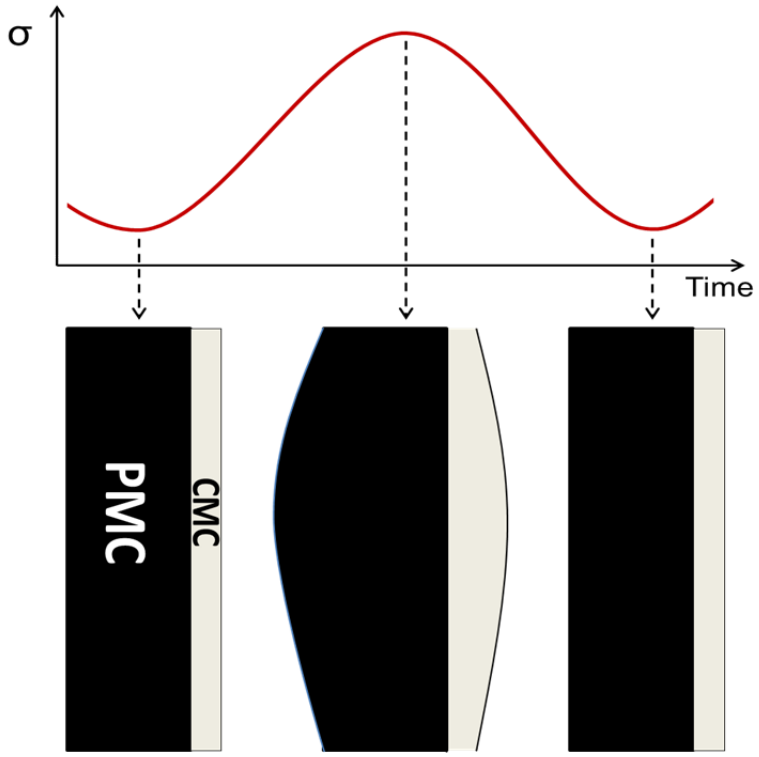

Figure 40. Schematic of non-homogeneous deformation during tension-tension cyclic loading. Individual plies are not shown. [17]

Figures 41 and 42 show MS4 0/90 specimen that failed in tension-tension fatigue test with σ_{max} of 430 MPa. Note that the specimen broke in two parts upon failure. Delamination of PMC plies is clearly visible as is the separation of the CMC and PMC

parts in the vicinity of the fracture location. Matrix cracks in the PMC part often extend from the gage section into the gripping sections of the specimen.

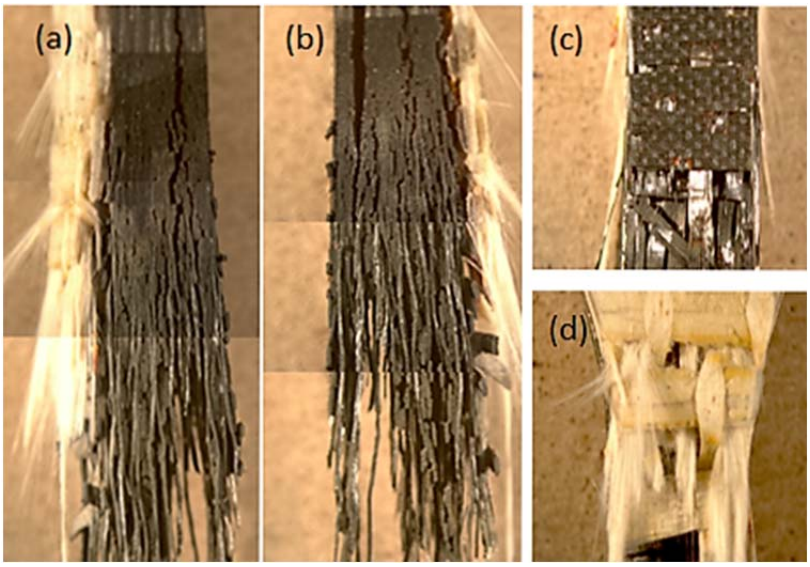

Figure 41. Stitched optical micrograph of the MS4 0/90˚ specimen T7-4 after failure under tension-tension fatigue at 430 MPa: (a) Front, (b) back, (c) left, (d) right.

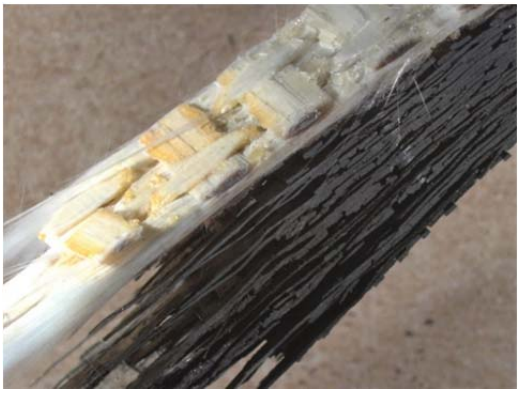

Figure 42. Optical micrograph of specimen T7-4 viewed from an angle after failure under tension-tension fatigue at 430 MPa.

5.6.2 Examination of the MS4 specimens with ±45 fiber orientation.

Figure 43 shows the gage section of as-processed MS4 specimen T8-7 with ±45˚ fiber orientation. Matrix voids are seen, but not as many as in the 0/90° specimens. In fact, the panel cut into ±45 specimens was slightly smoother than the panel cut into 0/90°. It also showed fewer major flaws.

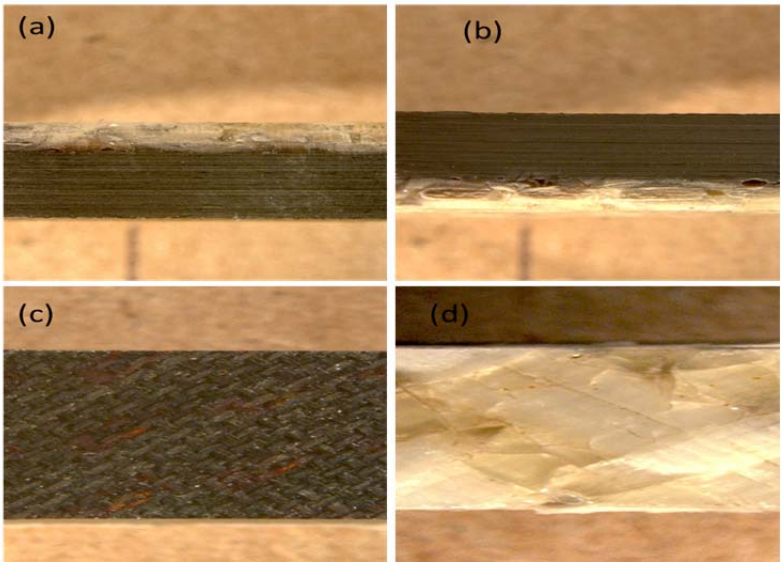

Figure 43. Optical micrographs of as-processed MS4 specimen with ±45° fiber orientation (T8-7): (a)-(b) side views, (c) PMC face, (d) CMC face.

Figure 44 shows stitched optical micrographs of the specimen T8-6 subjected to tension-to-failure test and specimen T8-10 failed in tension test after surviving $2x10^5$ fatigue cycles with maximum stress of 43 MPa. Failures of the two specimens have similar appearance and both are localized in the specimen gage section.

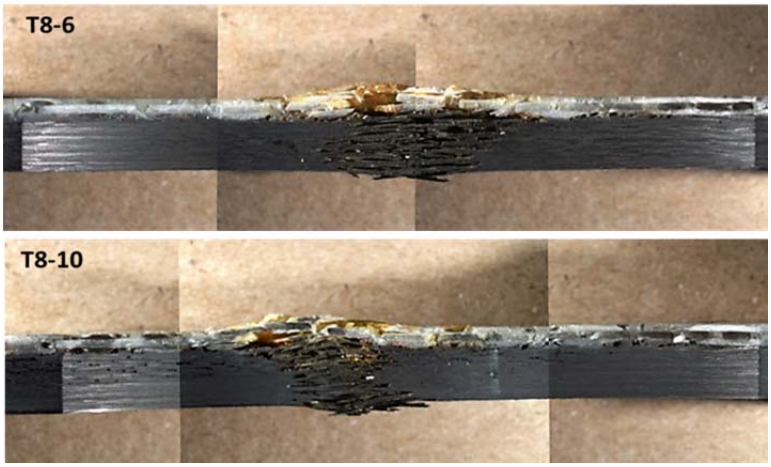

Figure 44. Stitched optical micrographs of the MS4 ±45° specimens T8-6 and T8-10 after failure in tension at elevated temperature.

Figures 45 and 46 show the stitched micrographs of the ±45 specimen tested in tension-tension fatigue at 76 MPa. Note the "scissoring" effect - fibers detach from the matrix material and align in the direction of the applied load. Delamination of the PMC part is evident. However, ply delamination and severe damage were confined to the specimen gage section. Additional optical micrographs are provided in the Appendix C.

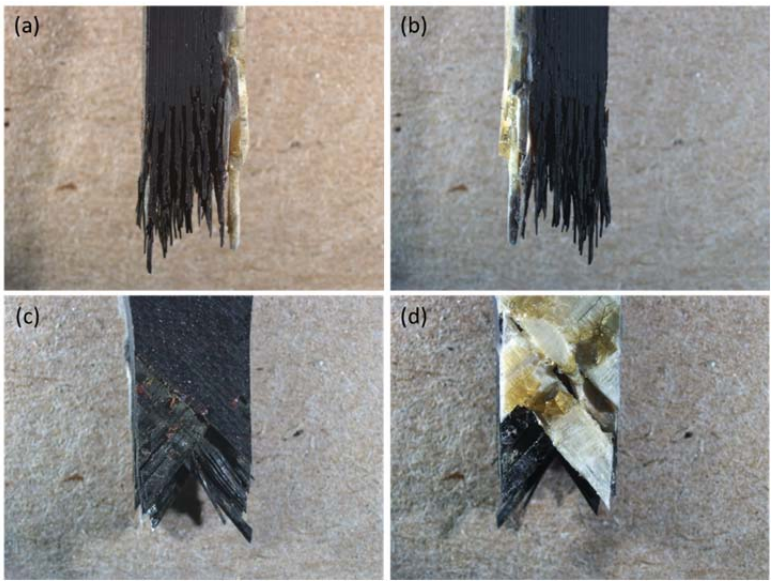

Figure 45. Optical micrograph of the MS4 ±45˚ specimen T8-1 after failure in tension-tension fatigue at 76 MPa: (a)-(b) side views, (c) PMC face, (d) CMC face.

Figure 46. Optical micrograph of specimen T8-1 viewed from an angle after failure in tension-tension fatigue at 76 MPa.

VI. Conclusion and Recommendations

6.1 Concluding Remarks

This research effort examined the tensile stress-strain behavior and tensile properties of the unitized composite MS4 (2D PMC/ 3D CMC) for both 0/90˚ and ±45° fiber orientations at elevated temperature. As expected, the 0/90˚ specimens presented significantly higher UTS and modulus values than the ±45° specimens. The tensile properties obtained for MS4 were also compared to the results reported by Wilkinson [3] for other similar material systems - the MS2 (2D PMC) and the MS3 (2D PMC/2D CMC). For the 0/90° fiber orientation, the MS4 exhibited lower UTS and modulus than the MS2 or the MS3 composites. The failure strain was nearly the same for the three material systems. For the ±45° fiber orientation, the MS2 exhibited higher strength and stiffness, and significantly greater failure strain than the MS4 unitized composite. Conversely, the MS4 showed higher UTS, slightly lower modulus and greater failure strain than the MS3. Apparently the use of the 3D fiber architecture in the CMC part served to improve the tensile strength of the unitized composite.

The tension-tension fatigue performance of the unitized 2D PCM/3D CMC material system was investigated at elevated temperature for both fiber orientations. As expected, the ±45° specimens showed a limited fatigue performance and load bearing capability compared to the 0/90° specimens. Furthermore, it is noted that the fatigue performance of the MS2 was significantly better than that of the MS4 for both fiber orientations. Likewise, fatigue performance of the MS3 with 0/90 fiber orientation was considerably better than the fatigue performance of the MS4 with 0/90 fiber orientation.

However, the MS4 presented better fatigue performance than the MS3 for the ±45° fiber orientation.

The use of 3D fiber architecture improves delamination resistance of the CMC of MS4. However, the MS4 specimens exhibit extensive delamination of the PMC plies during tensile tests and tension-tension fatigue test. We conclude that the MS4 material systems offer only marginal improvement in the overall delamination resistance. Furthermore, the MS4 exhibits lower tensile strength and stiffness and offers reduced fatigue performance compared to the previously studied MS2 and MS3 material systems.

6.2 Recommendations

For future work, it is recommended to conduct additional tests to better understand the mechanical behavior of the MS4 unitized composite. The following aspects of material behavior can be investigated:

- Effect of frequency on tension-tension fatigue.
- Failure initiation and progression during tension-tension fatigue loading.
- Mechanical behavior under complex operating environments including higher temperature and moisture.
- Compressive properties and tension-compression fatigue performance.

Finally, it may be beneficial to extend the 3D weave architecture to the PMC portion of the unitized composite.

Appendix A: Description of the compared material systems

The description of material systems is as written by Wilkinson and as provided by the manufacturer.

A.1 Material System 2: 2D Weave PMC

This material system consists of the NRPE matrix reinforced with 15 plies of 2D carbon de-sized Cytec T650-35 fibers woven in an 8 harness satin weave. The method of fabrication was prepreg [3].

A.2 Material System 3: 2D Weave Unitized Composite

This material system is a unitized composite consisting of a PMC and a thin CMC layer. Both the PMC and the CMC are reinforced with a 2D fabric with an 8 harness satin weave. However, the matrix and reinforcement materials differ. The PMC side utilizes the same material and fiber fabric pattern as MS2, but has only 12 plies; whereas the CMC portion has 3 plies of 2D fabric, made of 1059 HT sized JPS Astroquartzr III 4581. The ceramic matrix, C5 developed by P^2SI®, was produced by blending KDT HTT-1800 polysilazane-based pre-ceramic resin with yttria-stabilized zirconia and silica additives. The method of fabrication was prepreg [3].

Appendix B: Additional Fatigue plots

Stress-strain hysteresis responses for the remaining MS4 specimens are given in the following Figures.

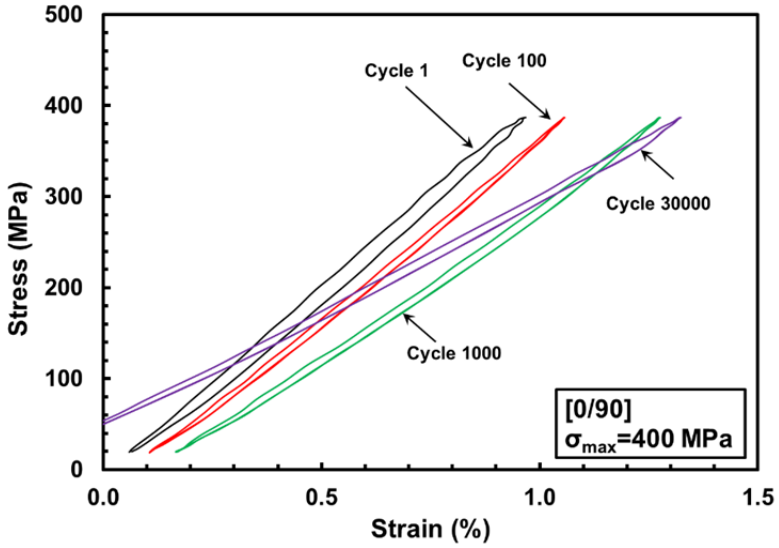

Figure 47. Evolution of stress-strain hysteresis response with fatigue cycles for specimen T7-17 of the MS4 with 0/90° fiber orientation at elevated temperature.

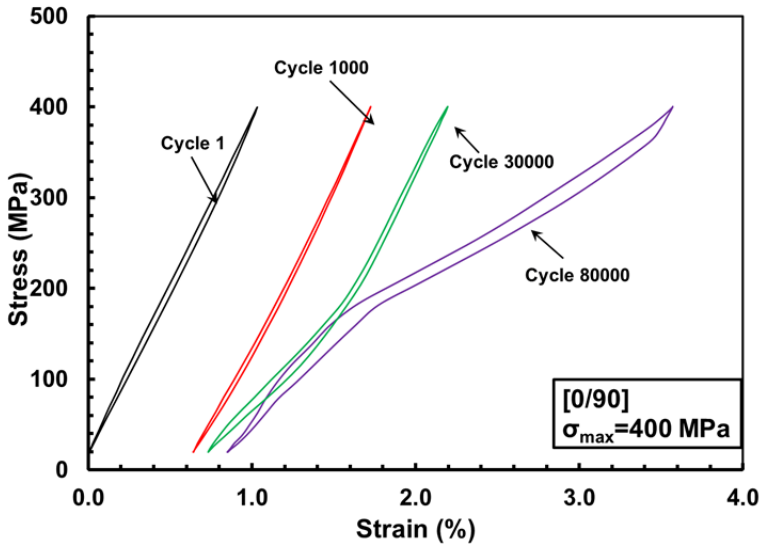

Figure 48. Evolution of stress-strain hysteresis response with fatigue cycles for specimen T7-19 of the MS4 with 0/90° fiber orientation at elevated temperature.

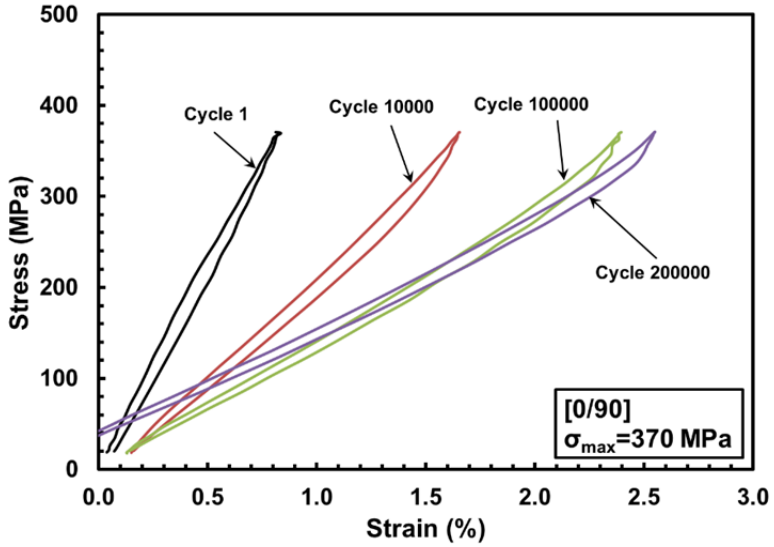

Figure 49. Evolution of stress-strain hysteresis response with fatigue cycles for specimen T7-14 of the MS4 with 0/90° fiber orientation at elevated temperature.

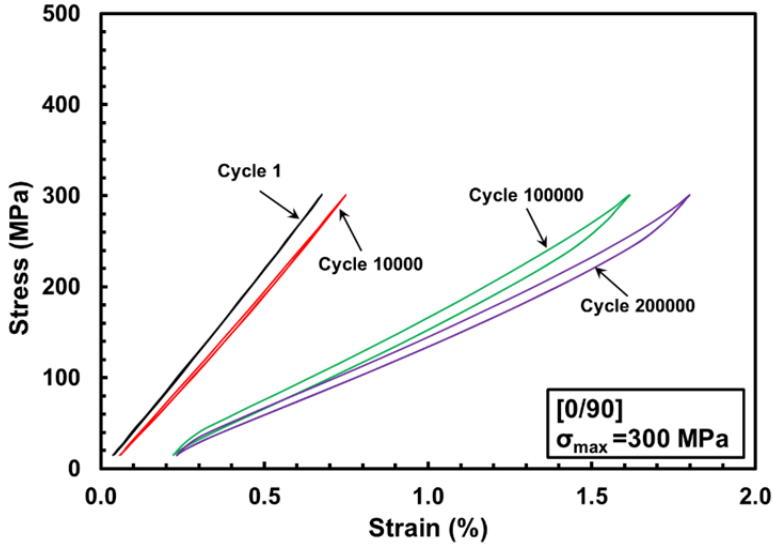

Figure 50. Evolution of stress-strain hysteresis response with fatigue cycles for specimen T7-7 of the MS4 with 0/90° fiber orientation at elevated temperature.

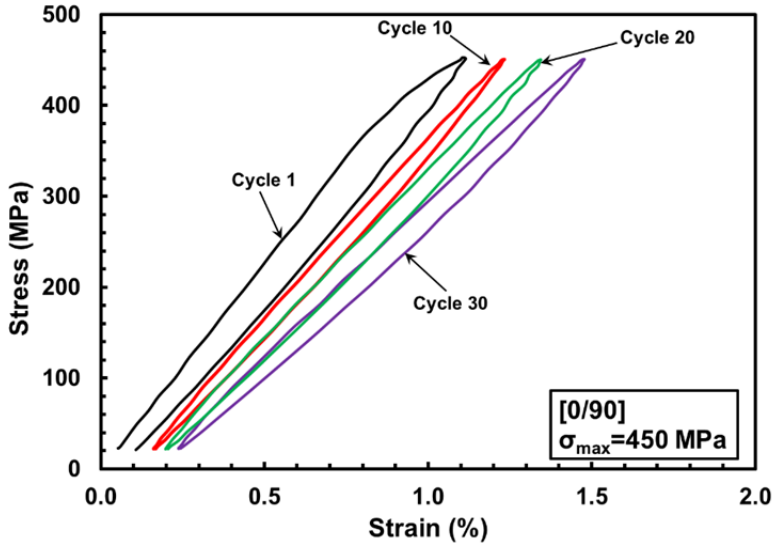

Figure 51. Evolution of stress-strain hysteresis response with fatigue cycles for specimen T7-12 of the MS4 with 0/90° fiber orientation at elevated temperature.

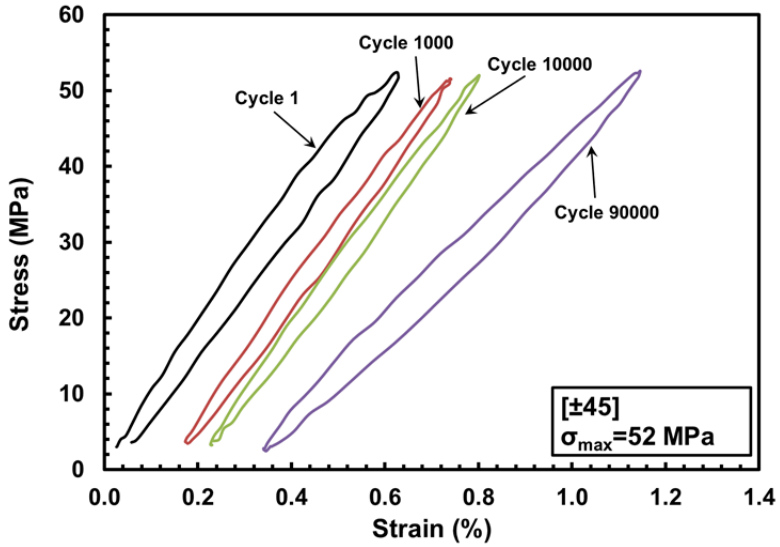

Figure 52. Evolution of stress-strain hysteresis response with fatigue cycles for specimen T8-14 of the MS4 with ±45° fiber orientation at elevated temperature.

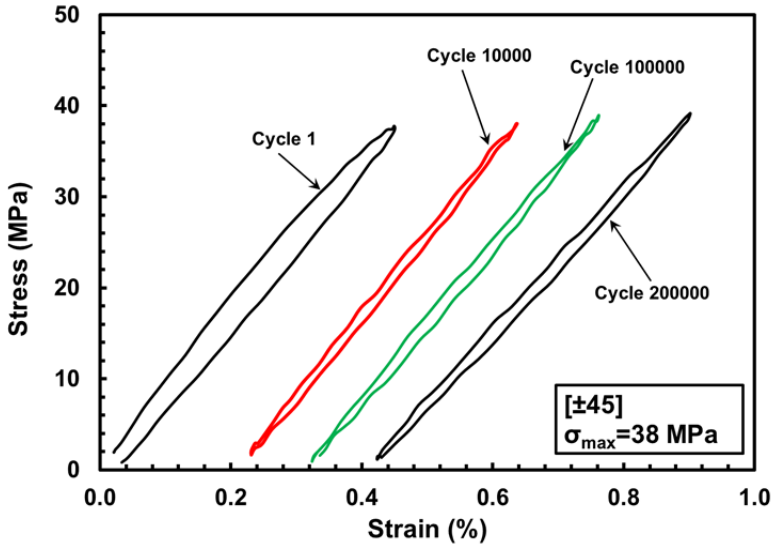

Figure 53. Evolution of stress-strain hysteresis response with fatigue cycles for specimen T8-9 of the MS4 with ±45° fiber orientation at elevated temperature.

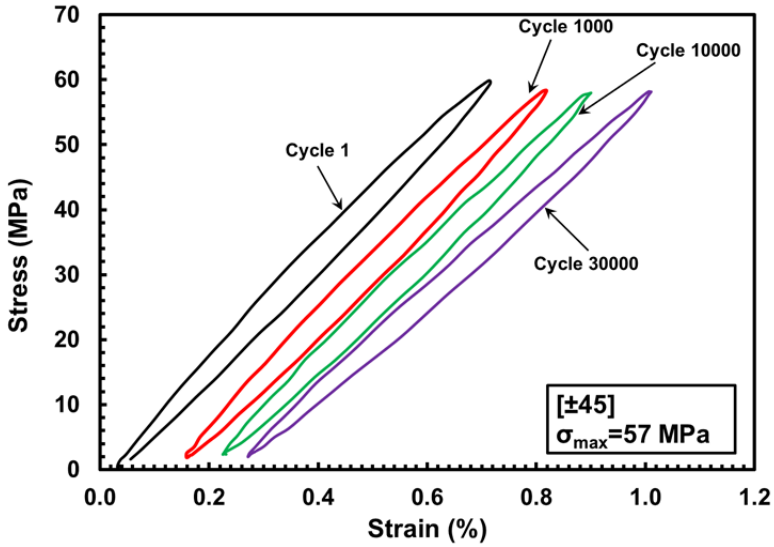

Figure 54. Evolution of stress-strain hysteresis response with fatigue cycles for specimen T8-7 of the MS4 with ±45° fiber orientation at elevated temperature.

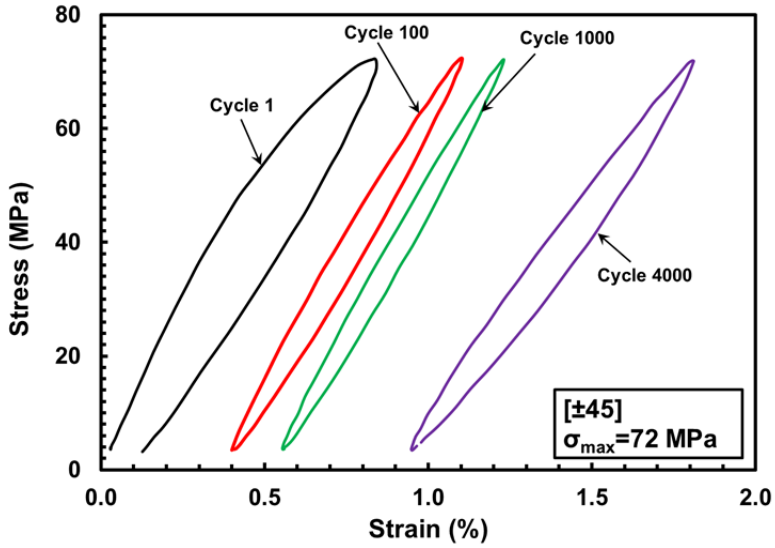

Figure 55. Evolution of stress-strain hysteresis response with fatigue cycles for specimen T8-2 of the MS4 with ±45° fiber orientation at elevated temperature.

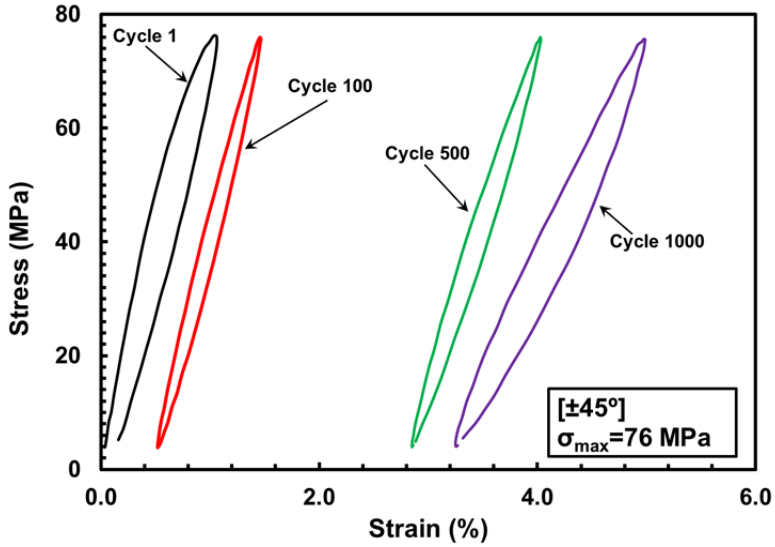

Figure 56. Evolution of stress-strain hysteresis response with fatigue cycles for specimen T8-1 of the MS4 with ±45° fiber orientation at elevated temperature.

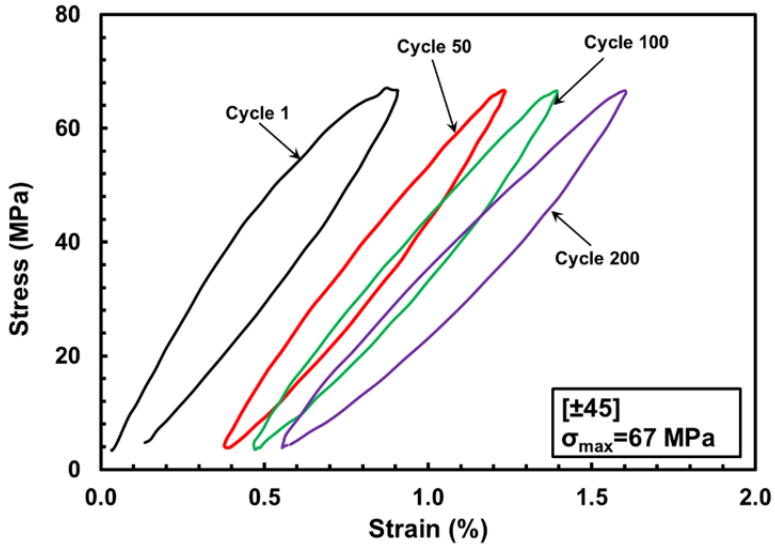

Figure 57. Evolution of stress-strain hysteresis response with fatigue cycles for specimen T8-3 of the MS4 with ±45° fiber orientation at elevated temperature.

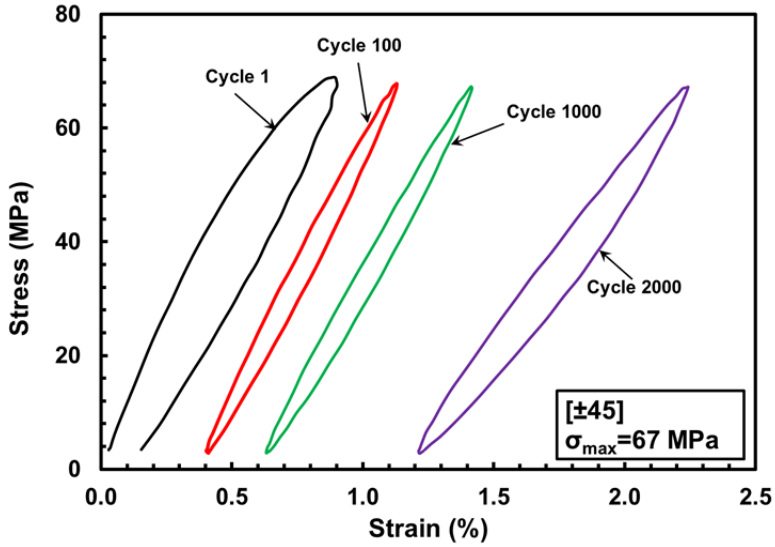

Figure 58. Evolution of stress-strain hysteresis response with fatigue cycles for specimen T8-12 of the MS4 with ±45° fiber orientation at elevated temperature.

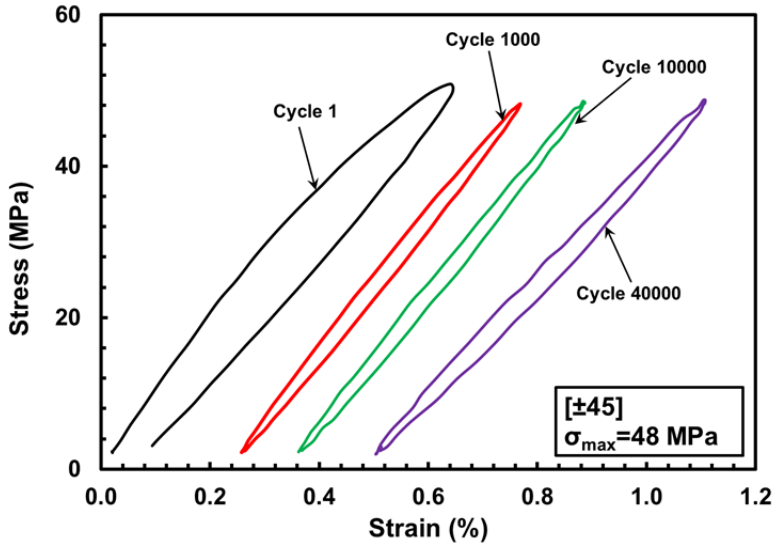

Figure 59. Evolution of stress-strain hysteresis response with fatigue cycles for specimen T8-8 of the MS4 with ±45° fiber orientation at elevated temperature.

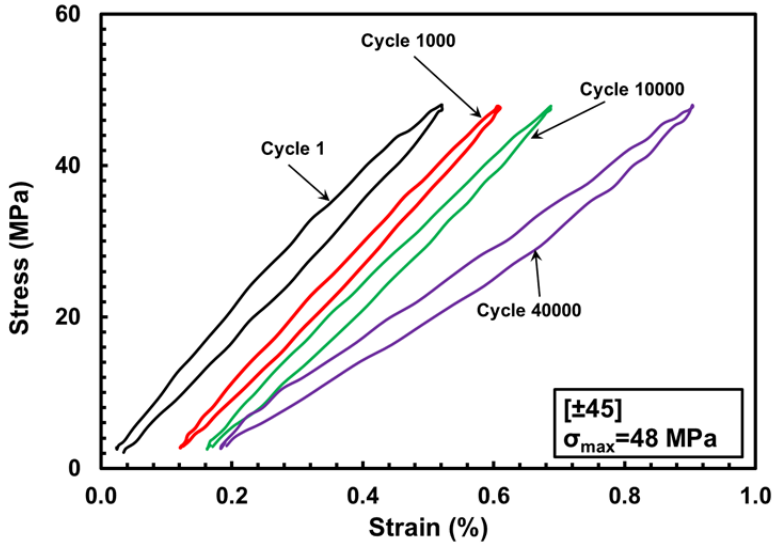

Figure 60. Evolution of stress-strain hysteresis response with fatigue cycles for specimen T8-11 of the MS4 with ±45° fiber orientation at elevated temperature.

Appendix C: Additional Optical images

More typical optical micrographs for the MS4 specimens are given in the current Appendix.

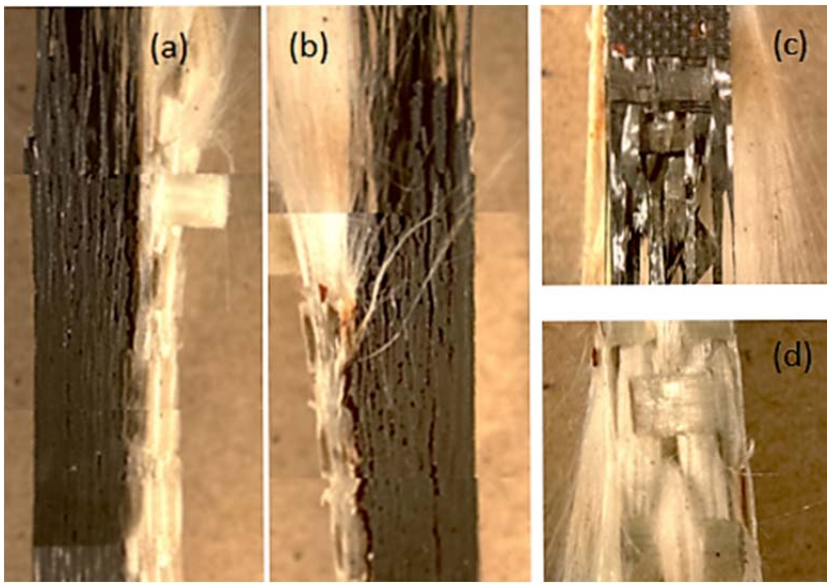

Figure 61. Stitched optical micrograph of the MS4 0/90˚ specimen T7-12 after failure under tension-tension fatigue at 450 MPa: (a) Front, (b) back, (c) left, (d) right.

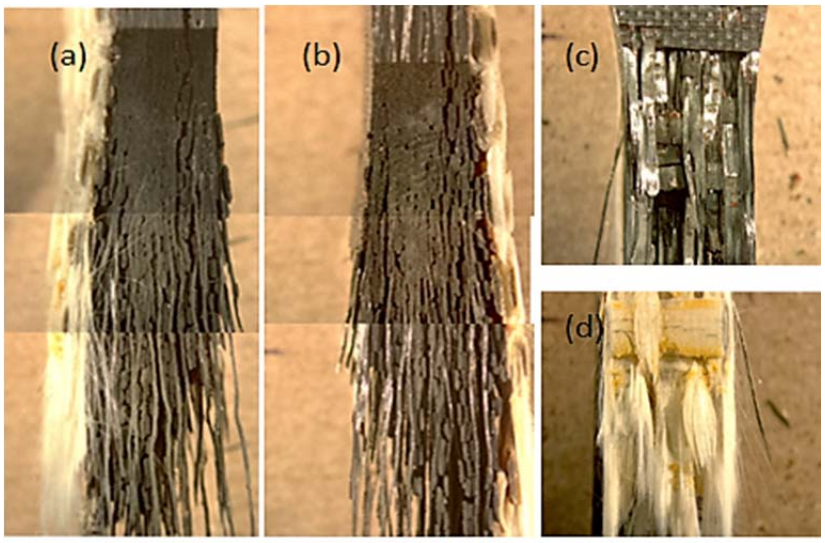

Figure 62. Stitched optical micrograph of the MS4 0/90˚ specimen T7-20 after failure under tension-tension fatigue at 420 MPa: (a) Front, (b) back, (c) left, (d) right.

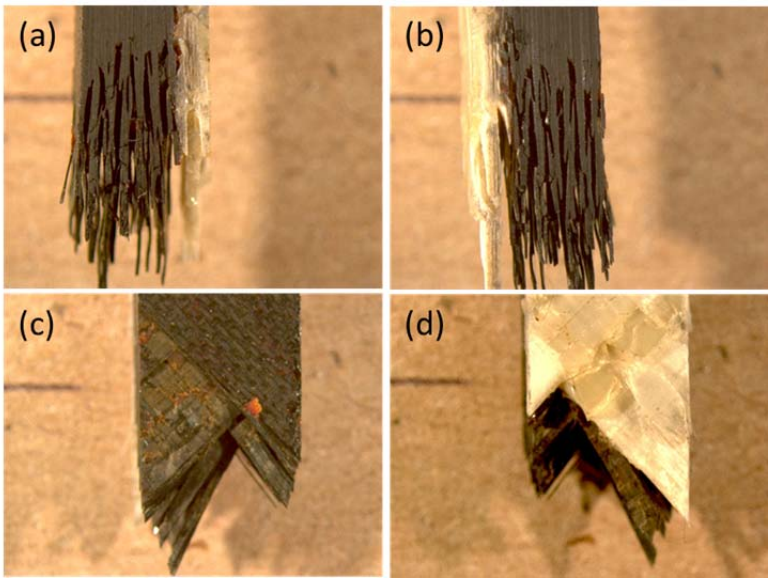

Figure 63. Optical micrograph of the MS4 ±45˚ specimen T8-2 after failure under tension-tension fatigue at 72 MPa: (a) Front, (b) back, (c) left, (d) right.

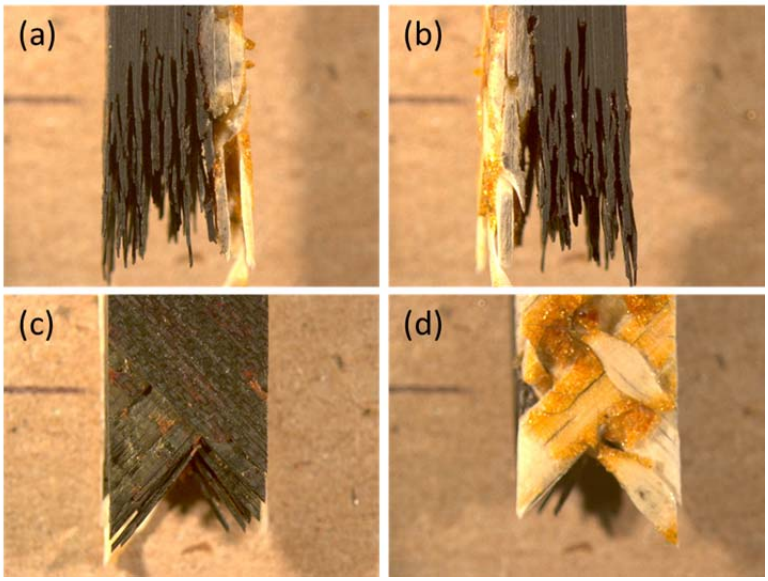

Figure 64. Optical micrograph of the MS4 ±45˚ specimen T8-13 after failure under tension-tension fatigue at 62 MPa: (a) Front, (b) back, (c) left, (d) right.

Bibliography

1. United States Department of the Air Force. “Materials in the Current Air Force”. http://www.au.af.mil/au/awc/awcgate/vistas/match3.pdf [Online; accessed 4 Apr 2016].

2. Stig, Fredrik. “3D-Woven Reinforcement in Composites”. Ph.D. thesis, KTH School of Engineering Sciences, Stockholm, Sweden, 2012.

3. Wilkinson, M. “Mechanical Properties and Fatigue Behavior of Unitized Composite Airframe Structures at Elevated Temperature”. Master’s thesis, Air Force Institute of Technology, Wright-Patterson AFB, Ohio, 2013.

4. Alnatifat Saleh, A. “Tension-compression fatigue behavior of 2D and 3D polymer matrix composites at elevated temperature”. Master’s thesis, Air Force Institute of Technology, Wright-Patterson AFB, Ohio, 2015.

5. F.C. Campbell. “Structural Composite Materials” ASM International®, Materials Park, Ohio 44073-0002, www.asminternational.org.

6. Daniel, Isaac M. and Ori Ishai. “Engineering Mechanics of Composite Materials”. Oxford University Press, New York, NY, 2nd edition, 1994.

7. Koide, R., De Franco, G., and Luerson, M. “An ant colony algorithm applied to lay up optimization of laminated composite plates”. Latin American Journal of Solids and Structures, May 2012.

8. U.S Congress, Office of Technology Assessment, Advanced Materials by Design, OTA-E-351 (Washington, DC: U.S. Government Printing Office, June 1988).

9. Chawla, K. K. “Ceramic Matrix Composites”. Kluwer Academic Publishers, Norwell,MA, 2nd edition, 2003

10. J. G. Sun, C. M. Deemer, W. A. Ellingson, and J. Wheeler Energy. “NDE Technologies for Ceramic Matrix Composites: Oxide and Non-Oxide”. Technology Division Argonne National Laboratory, Argonne, IL 60439.

11. Stig, Fredrik. “3D-Woven Reinforcement in Composites”. Ph.D. thesis, KTH School of Engineering Sciences, Stockholm, Sweden, 2012.

12. Anthony M. Waas. “The Development of a Shock Tube Facility for Studying the Blast Response of Textile Composite Laminates”. Composite Structures Laboratory, 2008

13. Carrillo, J.G. and W.J. Cantwell. “Mechanical properties of a novel fiber—metal laminate based on a polypropylene composite”. Mechanics of Materials, 41(7):828 –838, 2009. ISSN 0167-6636.

14. Lincoln, Jason E. “NRPE Composite Materials”. http://www.p2si.com/prepregs/datasheets/NRPE-Public-Release.pdf.

15. Starfire® Systems. “StarPCS™ SMP-730”. http://www.starfiresystems.com/docs/ceramic-forming-polymers/SMP-730.pdf

16. David Hartman, Mark E. Greenwood, and David M. Miller. “High Strength Glass Fibers”. AGY® http://www.agy.com/wpcontent/uploads/2014/03/High_Strength_Glass_Fibers-Technical.pdf

17. M. B. Ruggles-Wrenn and M. P. Wilkinson, “Fatigue of 2D and 3D Carbon-Fiber-Reinforced Polymer Matrix Composites and of a Unitized Polymer/Ceramic Matrix Composite at Elevated Temperature”, Fifty Years of Progress in Carbon Fiber Research, P. W. R. Beaumont, C. Soutis, A. Hodzic, eds., Springer, in press.

REPORT DOCUMENTATION PAGE

Form Approved
OMB No. 074-0188

1. REPORT DATE *(DD-MM-YYYY)*	**2. REPORT TYPE**	**3. DATES COVERED** *(From – To)*
18-08-2016	Master's Thesis	September 2014 – September 2016

TITLE AND SUBTITLE

Mechanical Properties and Fatigue Behavior of Unitized Composite Airframe Structures at Elevated Temperature

5a. CONTRACT NUMBER

5b. GRANT NUMBER

5c. PROGRAM ELEMENT NUMBER

6. AUTHOR(S)

Mohamed Noomen, Lieutenant, TNAF

5d. PROJECT NUMBER

5e. TASK NUMBER

5f. WORK UNIT NUMBER

7. PERFORMING ORGANIZATION NAMES(S) AND ADDRESS(S)
Air Force Institute of Technology
Graduate School of Engineering and Management (AFIT/ENY)
2950 Hobson Way, Building 640
WPAFB OH 45433-8865

8. PERFORMING ORGANIZATION REPORT NUMBER

AFIT-ENY-16-S-066

9. SPONSORING/MONITORING AGENCY NAME(S) AND ADDRESS(ES)
Air Force Research Laboratory/RQVS
Mr. Michael Falugi
2790 D Street, Bldg. 65
WPAFB OH 45433-7402
(937) 656-8810 michael.falugi@us.af.mil

10. SPONSOR/MONITOR'S ACRONYM(S)

AFRL/RQVS

11. SPONSOR/MONITOR'S REPORT NUMBER(S)

12. DISTRIBUTION/AVAILABILITY STATEMENT
DISTRUBTION STATEMENT A**.** APPROVED FOR PUBLIC RELEASE; DISTRIBUTION UNLIMITED.

13. SUPPLEMENTARY NOTES
This material is declared a work of the U.S. Government and is not subject to copyright protection in the United States.

14. ABSTRACT
The tension-tension fatigue behavior of a newly developed unitized composite material system was investigated. The unitized composite consisted of a polymer matrix composite (PMC) co-cured with a ceramic matrix composite (CMC). The PMC portion consisted of an NRPE high-temperature polyimide matrix reinforced with carbon fibers woven in an eight harness satin weave (8HSW). The CMC layer is a single-ply non-crimp 3D orthogonal weave composite consisting of ceramic matrix reinforced with glass fibers. In order to assess the performance and suitability of this composite for use in aerospace components designed to contain high-temperature environments, mechanical tests were performed under temperature conditions simulating the actual operating conditions. In all elevated temperature tests the CMC side of the test specimen was at 329°C while the PMC side was exposed to ambient laboratory air. The tensile properties were measured at elevated temperature for both on-axis [0/90] and off-axis [±45] fiber orientations. Tension-tension fatigue tests were conducted at elevated temperature at a frequency of 1.0 Hz with a ratio of minimum stress to maximum stress of R= 0.05

15. SUBJECT TERMS
Polymer Matrix Composites, Ceramic Matrix Composites, Unitized Composites, Fatigue, Mechanical Properties

16. SECURITY CLASSIFICATION OF:			**17. LIMITATION OF ABSTRACT**	**18. NUMBER OF PAGES**	**19a. NAME OF RESPONSIBLE PERSON**
a. REPORT	**b. ABSTRACT**	**c. THIS PAGE**			Dr. Marina B. Ruggles-Wrenn (ENY)
U	**U**	**U**	**UU**	87	**19b. TELEPHONE NUMBER** *(Include area code)* (937) 255-3636 x4641 marina.ruggles-wrenn@afit.edu

Standard Form 298 (Rev. 8-98)
Prescribed by ANSI Std. Z39-18